This is the Pre-Published Version.

The following publication L. F. Xie, I. W. Ho, S. C. Liew, L. Lu and F. C. M. Lau, "The Feasibility of Mobile Physical-Layer Network Coding with BPSK Modulation," in IEEE Transactions on Vehicular Technology, vol. 66, no. 5, pp. 3976-3990, May 2017 is available at https://doi.org/10.1109/TVT.2016.2602369

The Feasibility of Mobile Physical-Layer Network Coding with BPSK Modulation

Ling Fu Xie, Ivan Wang-Hei Ho, *Member, IEEE,* Soung Chang Liew, *Fellow, IEEE,* Lu Lu, *Member, IEEE,* and Francis C. M. Lau, *Senior Member, IEEE,*

***Abstract*—This paper considers applying Physical-layer Network Coding (PNC) to OFDM modulated Mobile Ad-hoc Networks (MANETs) to resolve the outstanding issue of short contact time between nodes due to their mobility. Ideally, PNC enables data exchange twice faster than traditional scheduling and thus, it is a potential performance booster in MANETs. However, application of PNC in MANETs is challenged by the carrier frequency offset (CFO) problem inherently caused by node-motion induced Doppler shifts and asynchronous oscillators. CFO induces inter-carrier interference (ICI) that degrades PNC performance. In this paper, we investigate the CFO/ICI impact on the signal-to-interference-and-noise ratio (SINR) and bit error rate (BER) in the signal detection of PNC in a two-way relay channel (TWRC) based on BPSK modulation. We find that PNC with power control suffers at most 3 dB SINR penalty compared with generic point-to-point communications in both the flat fading and the frequency-selective channels. Also, we find that a belief propagation (BP) algorithm could be employed in the signal detection of PNC to effectively tackle ICI and reduce its impact on the BER of PNC. For CFO compensation in PNC, we propose a method that amounts to positioning the relay's local oscillator frequency at the middle of the received frequencies from the two end nodes in the TWRC. Importantly, we show that (i) this compensation method can theoretically maximize the worst SINR in PNC; and (ii) in case of similar CFO of the two uplinks in TWRC, it allows PNC to achieve a BER at the relay close to that in the ideal case, i.e., in point-to-point communications without CFO. Overall, this paper demonstrates that mobile PNC is feasible in general, laying the foundation for future studies.**

***Index Terms*—Mobile ad-hoc networks, physical-layer network coding, carrier frequency offset, belief propagation.**

Copyright (c) 2015 IEEE. Personal use of this material is permitted. However, permission to use this material for any other purposes must be obtained from the IEEE by sending a request to pubs-permissions@ieee.org.

L. F. Xie is with the Faculty of Electrical Engineering and Computer Science, Ningbo University, Ningbo, China (e-mail: xiel0002@ntu.edu.sg).

I. W.-H. Ho and F. C.M. Lau are with the Department of Electronic and Information Engineering, The Hong Kong Polytechnic University, Hong Kong; and The Hong Kong Polytechnic University Shenzhen Research Institute, China (e-mail: {ivanwh.ho, encmlau}@polyu.edu.hk).

S. C. Liew is with the Department of Information Engineering, and L. Lu is with the Institute of Network Coding, The Chinese University of Hong Kong, Hong Kong (e-mail: {soung, lulu}@ie.cuhk.edu.hk).

This work was supported in part by the Early Career Scheme (Project No. 25200714) established under the University Grant Committee (UGC) of the Hong Kong Special Administrative Region (HKSAR), China; by the National Natural Science Foundation of China (NSFC, Project No. 61401384); and by The Hong Kong Polytechnic University (Projects G-YBK6, G-YN17, 4-ZZCZ). The contribution of L. F. Xie to this work was supported by the NSFC (Project No. 61601254 and 61571250). The contribution of S. C. Liew to this work was supported by the General Research Funds (Project No. 414713) and the contribution of L. Lu was supported by the AoE grant E-02/08, established under the UGC of the HKSAR, China. The contribution of F. C. M. Lau to this work was supported by the NSFC (Project No. 61372095).

I. Introduction

MOBILE Ad-hoc Network (MANET) has been a hot research topic for decades. Owing to its self-organizing attribute, it has wide applications in practice, e.g., in transportation systems [1], underwater exploration [2], etc. In MANETs, an outstanding issue is the relatively short contact duration between nodes due to their mobility, which may cause an established route to break frequently. In Vehicular Ad-hoc Networks (VANETs), for example, [3] showed that the average contact duration between buses in an inter-bus communication network in urban area is only about 47 sec. Hence, given an increasing demand of data exchange, e.g., in streaming of multimedia, to utilize the limited contact duration to transmit as much data as possible is challenging and critical to MANETs. This paper studies this issue for OFDM modulated MANETs, as OFDM has gained popularity in various applications of MANETs, including the standardized VANETs by 802.11p [4] and underwater ad-hoc networks [5].

Physical-layer Network Coding (PNC) is a promising technique that has found great success in relay networks [6]. MANET is a multihop network where relay scenarios are often seen: Fig. 1 shows a representative relay scenario within MANET, where two end nodes, nodes A and B, exchange packets X_A and X_B via a relay R in the middle. The network of Fig. 1 is named Two-Way Relay Channel (TWRC). For the packet exchange in TWRC, the traditional scheduling (TS) based on point-to-point transmissions requires four time slots, while PNC requires only two time slots [6], corresponding to the following two phases

- The uplink phase of PNC (time slot 1): the two end nodes A and B transmit their packets X_A and X_B to the relay R simultaneously.
- The downlink phase of PNC (time slot 2): from the received overlapped signals of nodes A and B, relay R first performs XOR decoding, i.e., *decodes* a network-coded packet $X_R = X_A \oplus X_B$ using XOR, and then broadcasts X_R back to A and B.

Node A (B) then decodes its desired packet X_B (X_A) from the received packet X_R and its previously sent packet X_A (X_B) using $X_R \oplus X_A$ ($X_R \oplus X_B$). This way, PNC doubles the overall throughput of TWRC compared with TS, and could potentially solve the problem of the limited contact duration in MANETs.

We remark that there is a similar scheme called Analog Network Coding (ANC) proposed for relay networks [7]. In TWRC, ANC differs from PNC in the downlink transmission

© 2016 IEEE. Personal use of this material is permitted. Permission from IEEE must be obtained for all other uses, in any current or future media, including reprinting/republishing this material for advertising or promotional purposes, creating new collective works, for resale or redistribution to servers or lists, or reuse of any copyrighted component of this work in other works.

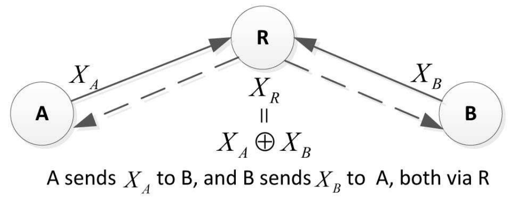

Fig. 1. A relay scenario in MANETs for PNC to be applied.

phase. Instead of decoding the overlapped signal, the relay in ANC simply *amplifies* the signal and then broadcasts it. The signal detection in ANC is only performed at the end nodes. In general, PNC (ANC) outperforms ANC (PNC) in TWRC when the uplinks are good (bad) and the downlinks are bad (good), meaning that neither of the two schemes can outperform the other in all situations [8]. In this paper, we focus on studying PNC in MANETs.

For PNC to succeed in OFDM modulated MANETs, however, a critical challenge that needs to be addressed first is the carrier frequency offset (CFO) problem inherently caused by the Doppler shift due to node motion, plus the oscillator asynchrony as well. First, the node motion will inevitably introduce Doppler shift to the carrier frequency of the signal. For the transmit signal from the end node i, $i \in \{A, B\}$, to relay R in Fig. 1, the amount of frequency shift, $f_{d,i}$, depends on the relative velocity, v_i, between the two nodes, that is,

$$f_{d,i} = \frac{v_i}{c} f_{c,i} \tag{1}$$

where c is the speed of waves (e.g., EM waves, sound waves, etc.) and $f_{c,i}$ is the carrier frequency. Second, due to local oscillator (LO) asynchrony, the frequency generated at a receiver for signal downconversion may be different from that used for signal upconversion at the transmitter. This also causes CFO. Such CFO will cause inter-carrier interference (ICI) between subcarriers in OFDM, which is detrimental to network performance such as Bit Error Rate (BER) [9], [10].

There have been many studies on estimation and compensation of CFO [9], [11]. CFO could be estimated via training symbols, e.g., in the 802.11 frame [10]. For traditional single-user point-to-point communications, the CFO, if known, could be compensated at the receiver. For PNC, however, it is not possible to completely eliminate the effect of CFO at the relay because of signals from multiple users. Let us consider the uplink phase of PNC. Since relay R receives data from the two end nodes simultaneously, eliminating the CFO of one link will still leave behind the CFO of the other link, given different CFO values for the two uplinks in PNC. Therefore, whether the node motion and/or the LO asynchrony will ruin the signal reception and impair the XOR decoding at relay R in PNC remains unknown. This paper aims to address this issue and explore the physical-layer feasibility of PNC in MANETs with signal processing techniques to reduce the impact of CFO/ICI. Compared with our previous work [12], [13], the major contributions of this paper are summarized as follows.

- First, we study how the CFO impacts the worst SINR among subcarriers at the relay in the uplink phase of PNC under both the flat fading channel and the frequency-selective channel. In both cases, our study shows that with power control there is at most 3 dB SINR penalty in PNC compared with traditional point-to-point communications.
- Second, we study the CFO impact on the BER of PNC at relay R based on BPSK modulation. Previous works [7], [10] generally treat the ICI as Gaussian noise for signal detection. For relatively high CFO in the uplink phase of PNC, however, we propose to use a belief propagation algorithm (BP) [14], [15] to address the ICI, and we show by simulation that with BP, the ICI effect on the BER of PNC could be effectively mitigated.
- Third, for CFO compensation in PNC, we propose a method that amounts to positioning the relay's LO frequency at the middle of the received frequencies from the two end nodes. Importantly, we show that (i) this method can theoretically maximize the worst SINR in PNC, and (ii) in case of similar CFO of the two uplinks in TWRC, it allows PNC to achieve a BER at relay R close to that in the ideal case, i.e., in point-to-point communications without CFO.

The rest of this paper is organized as follows. Section II gives the related work, and Section III describes the system model of our work. The impacts of CFO on the SINR and BER of PNC are presented in Sections IV and V, respectively. Then, the CFO compensation in PNC is studied in Section VI. Finally, Section VII concludes this paper.

II. Related Work

Since the seminal work of [6], PNC has attracted tremendous research attention in recent years. A comprehensive survey on PNC was given in [8], with a variety of issues in PNC studies covered and discussed. Here, we focus on the works and issues closely related to our study in this paper.

PNC as a performance booster for various networking functions in VANETs has been previously studied. [16] proposed the use of PNC for neighbor discovery in VANETs, and [17] proposed a MAC protocol for PNC in VANETs. However, these works neglected the CFO problem in PNC that motivates us to investigate the feasibility of PNC in MANETs/VANETs.

The relative phase offset between the signals of the end nodes is a critical issue in PNC. For single-carrier PNC, [18] and [19] analyzed the BER performance at relay R for BPSK and QAM modulations, respectively, both showing that the phase offset was detrimental to BER. Similar observation was made in [20] for QPSK modulation. In this paper, we study the joint effect of the phase offset and CFO in OFDM based PNC. We focus on BPSK modulation, but the extension to higher-order modulations, e.g., QPSK, is straightforward, as will be seen in Section V.

The relative symbol offset is another critical issue in PNC. For single-carrier PNC, [21] showed that the SINR penalty of this signal asynchrony was within 3 dB. However, [14] demonstrated that the symbol offset could be a reward to greatly mitigate the detrimental effect of the phase offset using BP in the signal detection of QPSK modulation. For OFDM based PNC in the frequency domain, if the cyclic prefix (CP) was longer than the maximal delay spread of the two uplinks, then the frequency-domain symbols stayed aligned and any time-domain symbol offset was simply translated into a phase offset for the frequency-domain symbols [10]. We assume a relatively long CP for OFDM in MANETs, and thus the symbol offset is not an issue in our study.

CFO is especially harmful to OFDM based PNC, as it destroys the orthogonality among subcarriers and thereby induces ICI. To deal with ICI, [5], [22], [23] explored iterative signal detection/decoding schemes at the relay in channel-coded PNC. In this paper, we study two signal detection schemes for unchannel-coded PNC, one treating ICI as Gaussian noise and the other employing BP, and particularly show the joint effect of the phase offset and CFO on the SINR and BER of PNC. We do not attempt to derive analytical BER expressions for the two schemes, as ICI is not Gaussian (as will be seen in Section V), posing difficulty for the derivation of a nice closed-form solution.

Channel estimation is also a key issue in PNC. For single-carrier PNC, [24] proposed a framework for joint channel estimation and decoding using both user data and pilots. For OFDM based PNC, [10] proposed a special 802.11 frame design that separated both the training symbols and frequency-domain pilots of the end nodes, allowing relay R to use conventional estimation methods (e.g., in [25]) to keep track of the two uplinks at the same time, including the channel gain functions and the CFO values.

Channel coding can be integrated into PNC to improve BER performance [8], [26]. Our work does not assume the use of channel coding, but it can be extended straightforwardly to incorporate channel coding, e.g., for a low-complexity extension, channel decoding at relay R can be performed on top of the XOR decoding or equivalently using the XOR-CD model in [8].

III. System Model

This paper considers applying PNC to OFDM modulated MANETs where a TWRC is formed, that is, two end nodes A and B want to exchange packets X_A and X_B via a relay R, as shown in Fig. 1. One inherent feature in Fig. 1 is that signals over every point-to-point link undergo carrier frequency offset (CFO), as detailed below.

We consider PNC in the frequency domain based on OFDM [10]. Let the number of subcarriers used in OFDM be K. Then the baseband OFDM signal transmitted by node i, $i \in \{A, B\}$, in one symbol duration T_s is represented in the time domain as

$$x_i(t) = \frac{1}{\sqrt{T_s}} \sum_{k=0}^{K-1} s_i[k] e^{j2\pi f_k t}, \qquad 0 < t \leq T_s \tag{2}$$

where $f_k = k\Delta_f$ is the frequency of the k-th subcarrier and $\Delta_f = 1/T_s$ is the subcarrier spacing, and $s_i[k]$ is the information of node i on the k-th subcarrier. Here, we assume BPSK modulation in OFDM, that is, $s_i[k] = +1$ for bit 0 and $s_i[k] = -1$ for bit 1. Also, we assume equal probabilities of transmitting bits 0 and 1 at each end node and the independence of the bits on all subcarriers.

We consider both the flat fading channel and the frequency-selective channel, and focus on the uplink phase of PNC. As mentioned earlier, thanks to the cyclic prefix (CP) in OFDM, the issue of time-domain symbol offset in PNC can be resolved [10], and we therefore assume in this study that symbols align in the frequency domain in both channel models. Furthermore, we assume that there is power control at the end nodes so that the received power levels for X_A and X_B at relay R are balanced, as elaborated below.

A. Power Control in PNC

Let $\gamma_{k,i}(t)$ be the channel gain function for the k-th subcarrier from node i to relay R at time t. Over the two phases of PNC in MANETs, we assume the magnitude, $|\gamma_{k,i}(t)|$, of $\gamma_{k,i}(t)$ keeps constant whereas its phase $\phi_{k,i}(t)$ varies. This assumption holds in 802.11p VANETs [1]. With the special OFDM frame design [10] as mentioned earlier, relay R in PNC can keep track of $\gamma_{k,A}(t)$ and $\gamma_{k,B}(t)$ at the same time. Then, through channel state information (CSI) feedback from relay R, node i can obtain $|\gamma_{k,i}(t)|$. Thus, we consider the following power control scheme for the TWRC system in our paper: node i multiplies the subcarrier signal to transmit with $1/|\gamma_{k,i}(t)|$. This scheme is analogous to the channel inversion based power control in [27] except that we do not pre-code the phase $\phi_{k,i}(t)$.

Our power control suits scenarios where nodes have ample energy and/or there is a line of sight (LOS) between node i and relay R. This can effectively mitigate the problem of the deep fading at some subcarrier(s) [27], e.g., in the frequency-selective channel. An example of such scenarios is VANETs, where a road-side unit acting as a relay is usually mounted high [1], thus providing LOS from vehicles to it.

If needed, the subcarrier suppression method [27] as an effective way to cope with the deep fading problem could be incorporated into our power control. We remark that with this method, the SINR analysis in Sections IV and VI may be affected, but the design of the signal detection schemes in Section V remains the same in principle. We leave the study of the subcarrier suppression as future work.

B. PNC under the Flat Fading Channel

For a flat fading channel from node i to relay R, the multipath channel gain has only one tap and all the subcarriers have the same channel gain function, denoted by $\gamma_i(t)$. With the proposed power control, the signal from node i, after passing through the channel, is

$$\widetilde{x}_i(t) = \gamma_i(t)\, x_i(t)\, \frac{1}{|\gamma_i(t)|} = e^{j\phi_i(t)}\, x_i(t) \tag{3}$$

where $\phi_i(t)$ is the phase of $\gamma_i(t)$.

Now let us start with point-to-point communications in the traditional scheduling (TS) to look at the received signal at

[1] Suppose the packet sent by node i or relay R has 1000 bytes, then it takes 2.67 ms for the two phases of PNC to complete, given 6 Mbps for BPSK bit rate in 802.11p [4]. Further suppose $v_i = 100$ km/h in (1), then the distance change between node i and relay R over the two phases of PNC is 7 cm, which is on the order of the 5.9 GHz wavelength (≈ 5 cm) in 802.11p and could cause $\phi_{k,i}(t)$ to vary but keep $|\gamma_{k,i}(t)|$ unchanged.

the relay for one OFDM symbol. Under an ideal condition without node mobility, the baseband signal $y_i(t)$ received at relay R from node i is given by

$$y_i(t) = e^{j\phi_i} x_i(t) + n(t) \tag{4}$$

where $n(t)$ is the white Gaussian noise with zero mean and variance σ^2. Note in (4) that without node mobility, $\phi_i(t)$ is a constant value equal to $\phi_i(0) = \phi_i$. Then, at relay R, the received signal $y_i(t)$ is multiplied with a bank of K correlators and integrated over the period T_s. The output at the m-th correlator ($0 \le m \le K-1$) is

$$y_i[m] = \frac{1}{\sqrt{T_s}} \int_0^{T_s} y_i(t) e^{-j2\pi f_m t} dt \tag{5}$$

Without CFO, it can be seen that only information sent through subcarrier m will be extracted at the m-th correlator, and information carried by other subcarriers $k \neq m$ will be eliminated.

However, node motion and/or local oscillator (LO) asynchrony could cause a mismatch between relay R's LO frequency and the carrier frequency of the received signal, which causes CFO that induces inter-carrier interference (ICI) among subcarriers, as shown below. Let the LO frequency of relay R (node i) for signal downconversion (upconversion) be $f_{o,R}$ ($f_{o,i}$). Here, $f_{o,i}$ is equivalent to $f_{c,i}$ in (1). Then, the overall CFO, f_{δ_i}, of the link from node i to relay R is approximately equal to $f_{d,i} + f_{o,i} - f_{o,R}$ [28], where $f_{d,i}$ is the Doppler shift in (1). Note that as mentioned earlier, f_{δ_i} can be estimated by relay R, e.g., using training symbols [10]. Here, we define the normalized CFO of f_{δ_i} as $\delta_i = f_{\delta_i}/\Delta_f$. With CFO considered, we have

$$y_i(t) = x_i(t)\, e^{j(2\pi f_{\delta_i} t + \phi_i)} + n(t) \tag{6}$$

Note that the Doppler shift $f_{d,i}$ that causes $\phi_i(t)$ to vary over t is now absorbed in f_{δ_i} in (6). Also, note in (6) that a narrowband MANET or a much higher carrier frequency $f_{c,i}$ relative to the bandwidth of $x_i(t)$ is assumed such that all subcarriers of node i undergo the same Doppler shift $f_{d,i}$. Substituting (2) and (6) into (5), we have

$$\begin{aligned} y_i[m] &= \frac{e^{j\phi_i}}{T_s} \sum\nolimits_k \{ \int_0^{T_s} s_i[k]\, e^{j2\pi(f_k - f_m + f_{\delta_i})t}\, dt \} + w_m \\ &= \frac{e^{j\phi_i}}{T_s} \sum\nolimits_k \{ s_i[k] \int_0^{T_s} e^{j2\pi(k-m+\delta_i)t/T_s} dt \} + w_m \end{aligned} \tag{7}$$

where $w_m = \frac{1}{\sqrt{T_s}} \int_0^{T_s} n(t) e^{-j2\pi f_m t} dt$ is the noise term at the m-th correlator. It can be found that the variance of w_m remains σ^2. Put $u = m - k$, and let

$$\begin{aligned} a_{u,i} &= \frac{1}{T_s} \int_0^{T_s} e^{-j2\pi(u-\delta_i)t/T_s} dt \\ &= \operatorname{sinc}(u - \delta_i)\, e^{-j\pi(u-\delta_i)} \end{aligned} \tag{8}$$

where $\operatorname{sinc}(x) = \frac{\sin(\pi x)}{\pi x}$. Here, $a_{u,i}$ represents the generation of the ICI from the k-th subcarrier on the m-th subcarrier, for $k \neq m$. Substituting (8) into (7), we have

$$y_i[m] = \underbrace{e^{j\phi_i} a_{0,i} s_i[m]}_{\text{signal}} + \underbrace{\sum\nolimits_{u\neq 0} e^{j\phi_i} a_{u,i} s_i[m-u]}_{\text{ICI}} + \underbrace{w_m}_{\text{noise}} \tag{9}$$

The first component on the RHS is the desired signal, and the second component corresponds to the ICI terms in the point-to-point case.

For PNC, the received signal $y_R(t)$ at relay R is the superposed signal from nodes A and B, i.e.,

$$y_R(t) = y_A(t) + y_B(t) + n(t) \tag{10}$$

Hence, the output, $y_R[m]$, of the m-th correlator at relay R after integration becomes

$$\begin{aligned} y_R[m] = &\underbrace{\sum_{i\in\{A,B\}} e^{j\phi_i} a_{0,i} s_i[m]}_{\text{desired signal}} \\ &+ \underbrace{\sum_{i\in\{A,B\}} \sum_{u\neq 0} e^{j\phi_i} a_{u,i} s_i[m-u]}_{\text{PNC\_ICI}} + \underbrace{w_m}_{\text{noise}} \end{aligned} \tag{11}$$

where the first term on the RHS is the desired signal, and the second term corresponds to the overall ICI for the m-th subcarrier in the PNC uplink phase. Thus, the relative phase offset between the desired signals of nodes A and B in (11) is given by $\Delta\theta = \phi_A - \phi_B + \pi(\delta_A - \delta_B)$, which applies to every subcarrier.

C. PNC under the Frequency-Selective Channel

For a frequency-selective channel, the multipath gain has multiple taps, with each tap associated with a channel gain and a time delay. The delay spread of the channel is defined as the maximal difference between these time delays. We assume in this paper that the delay spread of each channel in TWRC is within the CP length, yielding a flat fading for each subcarrier but different channel gains for different subcarriers [10], i.e., $\gamma_{k,i}(t)$ for the k-th subcarrier from node i. Applying the proposed power control to each individual subcarrier at node i, the m-th correlator output in TS with CFO considered is given by

$$y_i[m] = e^{j\phi_{m,i}} a_{0,i} s_i[m] + \sum\nolimits_{u\neq 0} e^{j\phi_{m-u,i}} a_{u,i} s_i[m-u] + w_m, \tag{12}$$

and the m-th correlator output in PNC is given by

$$\begin{aligned} y_R[m] = &\sum_{i\in\{A,B\}} e^{j\phi_{m,i}} a_{0,i} s_i[m] \\ &+ \sum_{i\in\{A,B\}} \sum_{u\neq 0} e^{j\phi_{m-u,i}} a_{u,i} s_i[m-u] + w_m \end{aligned} \tag{13}$$

Similar to (9), $\phi_{m,i}$ above is the phase of $\gamma_{m,i}(t)$ at $t = 0$.

IV. Impact of CFO on SINR in PNC

This section studies the effect of CFO in PNC on the SINR at the relay. We analyze the CFO effect based on the output of the correlators as given in (11) and (13).

A. SINR in PNC

We first define the SINR at one subcarrier in PNC. At the m-th correlator or subcarrier, from either (11) or (13) we find that (i) the power of the desired signal, $a_{0,i}s_i[m]$, from node i is given by $P_i[m] = |a_{0,i}|^2\mathrm{E}(|s_i[m]|^2) = \mathrm{sinc}^2(\delta_i)$, since $\mathrm{E}(|s_i[m]|^2) = 1$, and (ii) the power of the overall ICI term is given by $ICI_{pnc}[m] = \sum_{u\neq 0}\{|a_{u,A}|^2\,\mathrm{E}(|s_A[m-u]|^2) + |a_{u,B}|^2\,\mathrm{E}(|s_B[m-u]|^2)\} = \sum_{u\neq 0}\{\mathrm{sinc}^2(u-\delta_A)+\mathrm{sinc}^2(u-\delta_B)\}$. With (i) and (ii), the SINR at the m-th subcarrier in PNC is defined as follow:

$$SINR_{pnc}[m] = \frac{\min\{P_A[m], P_B[m]\}}{ICI_{pnc}[m] + \sigma^2} \tag{14}$$

where σ^2 is the variance of the noise w_m in (11) or (13). Under this definition, we see that for any subcarrier, the SINR values in our two considered channel models are the same. We have the following remark on the numerator in (14).

It is known that when performing XOR decoding in PNC at the relay, a smaller $P_i[m]$ generally means a shorter distance between two received constellation points decoded into different network-coded symbols, yielding higher BER [20]. Thus, with the numerator in (14) given by $\min\{P_A[m], P_B[m]\}$, our SINR can reflect the error performance more accurately.

For different m, $P_i[m] = \mathrm{sinc}^2(\delta_i)$ (or simply $P_i = \mathrm{sinc}^2(\delta_i)$) for both $i = A$ and B, and the variances of the noise w_m are the same. However, it can be seen that $ICI_{pnc}[m]$ may vary among different m. Hence, $SINR_{pnc}[m]$ varies with m. Here, we focus on the worst/lowest $SINR_{pnc}[m]$.

In this paper we assume $|\delta_i| < 0.5$, which can be regarded as the fractional CFO [29] and is sufficiently large in scenarios like VANETs [2]. Within this range of δ_i, Appendix A shows that the interference power, $ICI_{pnc}[m]$, at the *middle* subcarrier(s) in PNC is the largest, and thus the middle subcarrier(s) has the worst SINR. The worst SINR, denoted by $SINR^*_{pnc}$, is expressed as follows:

$$SINR^*_{pnc} = \begin{cases} \dfrac{\min\{P_A, P_B\}}{ICI_{pnc}[(K-1)/2] + \sigma^2}, & \text{for an odd } K \\ \min\{\dfrac{\min\{P_A, P_B\}}{ICI_{pnc}[K/2-1] + \sigma^2}, \dfrac{\min\{P_A, P_B\}}{ICI_{pnc}[K/2] + \sigma^2}\}, & \text{for an even } K \end{cases} \tag{15}$$

Note in (15) that for an even K, the worst SINR appears at either the $\frac{K}{2}$-th or $\frac{K-2}{2}$-th subcarrier, depending on the values of δ_A and δ_B (as will be shown below).

Case 1 in PNC: K is an odd number. Due to $P_i = \mathrm{sinc}^2(\delta_i)$, we see that for $-0.5 < \delta_i < 0.5$, P_i decreases as $|\delta_i|$ increases. Thus, we have

$$SINR^*_{pnc} = \begin{cases} \dfrac{P_A}{ICI_{pnc}[(K-1)/2] + \sigma^2}, & \text{for } |\delta_A| \geq |\delta_B| \\ \dfrac{P_B}{ICI_{pnc}[(K-1)/2] + \sigma^2}, & \text{for } |\delta_A| < |\delta_B| \end{cases} \tag{16}$$

Case 2 in PNC: K is an even number. We first determine the regions of (δ_A, δ_B) in which $ICI_{pnc}[K/2] \geq ICI_{pnc}[K/2-1]$. Appendix B shows that in regions 1 and 2 in Fig. 11 (i.e., when $\delta_B \geq -\delta_A$), we have $ICI_{pnc}[K/2] \geq ICI_{pnc}[K/2-1]$, and that in regions 3 and 4 (i.e., when $\delta_B < -\delta_A$), we have $ICI_{pnc}[K/2] < ICI_{pnc}[K/2-1]$. In particular, we further have $P_A \geq P_B$ in regions 1 and 3 and $P_A \leq P_B$ in the rest regions. Thus, we have

$$SINR^*_{pnc} = \begin{cases} \dfrac{P_B}{ICI_{pnc}[K/2] + \sigma^2}, & \text{for } \delta_B \geq |\delta_A| \\ \dfrac{P_A}{ICI_{pnc}[K/2] + \sigma^2}, & \text{for } \delta_A \geq |\delta_B| \\ \dfrac{P_B}{ICI_{pnc}[K/2-1] + \sigma^2}, & \text{for } \delta_B \leq -|\delta_A| \\ \dfrac{P_A}{ICI_{pnc}[K/2-1] + \sigma^2}, & \text{for } \delta_A \leq -|\delta_B| \end{cases} \tag{17}$$

In summary, for an odd K, $SINR^*_{pnc}$ always appears at subcarrier $\frac{K-1}{2}$, regardless of δ_A and δ_B, whereas for an even K, it appears at subcarrier $\frac{K}{2}$ when $\delta_B \geq |\delta_A|$ or $\delta_A \geq |\delta_B|$, and at subcarrier $\frac{K-2}{2}$ otherwise.

B. SINR in TS

Given either (9) or (12) for one point-to-point link in the traditional scheduling (TS), the SINR at the m-th subcarrier from node i is expressed as

$$SINR_i[m] = \frac{P_i}{ICI_i[m] + \sigma^2} \tag{18}$$

where $ICI_i[m] = \sum_{u\neq 0}\mathrm{sinc}^2(u-\delta_i)$ is the power of the ICI at the m-th subcarrier. Similar to $ICI_{pnc}[m]$ in PNC, $ICI_i[m]$ also varies with m, hence, we consider the worst $SINR_i[m]$ for fair comparison with PNC. Appendix A shows that the $ICI_i[m]$ at the middle subcarrier(s) is the largest, and thus the worst $SINR_i[m]$, denoted by $SINR^*_i$, among all subcarriers from node i also appears at the middle subcarrier(s), for $-0.5 < \delta_i < 0.5$. Specifically, for an odd K, $SINR^*_i = SINR_i[\frac{K-1}{2}]$; and for an even K, we have $SINR^*_i = SINR_i[\frac{K-2}{2}]$ when $\delta_i \leq 0$ and $SINR^*_i = SINR_i[\frac{K}{2}]$ when $\delta_i \geq 0$.

In case of $\delta_A \neq \delta_B$, we may have $SINR^*_A \neq SINR^*_B$. If $SINR^*_A$ ($SINR^*_B$) is lower, we would like to compare the link from node A (node B) with PNC, because that point-to-point link is the bottleneck in TS. Let $SINR^*_{ts}$ be $\min\{SINR^*_A, SINR^*_B\}$. In what follows, we determine $SINR^*_{ts}$ in different regions of (δ_A, δ_B).

Case 1 in TS: K is an odd number. Let us first consider an even function $f(x) = \mathrm{sinc}^2(u+x) + \mathrm{sinc}^2(u-x)$, where $u = 1, 2, 3, ...$ and $-0.5 < x < 0.5$. It can be seen that for any positive integer u, $f(x)$ increases as x increases from 0 to 0.5. Since $ICI_i[\frac{K-1}{2}]$ is equivalent

[2]In 802.11p VANETs, we have the center frequency $f_c = 5.9$ GHz and the subcarrier spacing $\Delta_f = 156.25$ kHz [12]. Assuming the relative velocity $v_i < 200$ km/h in (1), then the normalized Doppler shift $f_{d,i}$ is less than 0.008. Further, assuming the LO instability for 802.11 devices is within 3 parts per million (ppm, defined as $\frac{|f_o - f_c|}{f_c} \times 10^6$, where f_o is the actual LO frequency) [30], then the normalized $|f_{o,i} - f_{o,R}|$ is no more than 0.22, yielding $|\delta_i| < 0.23$.

to $\sum_{u=1}^{(K-1)/2}\{\text{sinc}^2(u+\delta_i)+\text{sinc}^2(u-\delta_i)\}$, we see that $ICI_i[\frac{K-1}{2}]$ increases as $|\delta_i|$ increases. Meanwhile, as mentioned earlier, P_i decreases as $|\delta_i|$ increases, hence a larger $|\delta_i|$ yields a lower $SINR_i^*$. Thus, we have

$$SINR_{ts}^* = \begin{cases} \dfrac{P_A}{ICI_A[(K-1)/2]+\sigma^2}, & \text{for } |\delta_A| \geq |\delta_B| \\ \dfrac{P_B}{ICI_B[(K-1)/2]+\sigma^2}, & \text{for } |\delta_A| < |\delta_B| \end{cases} \tag{19}$$

Case 2 in TS: K is an even number. First, Appendix B shows that in the four regions of (δ_A, δ_B) from 1 to 4 in Fig. 11, $ICI_B[\frac{K}{2}]$, $ICI_A[\frac{K}{2}]$, $ICI_B[\frac{K-2}{2}]$, and $ICI_A[\frac{K-2}{2}]$ are the largest among $ICI_i[m]$ for all i and m, respectively. Second, in Fig. 11 in Appendix B, we further have $P_B \leq P_A$ in regions 1 and 3 and $P_A \leq P_B$ in regions 2 and 4. Thus, we have

$$SINR_{ts}^* = \begin{cases} \dfrac{P_B}{ICI_B[K/2]+\sigma^2}, & \text{for } \delta_B \geq |\delta_A| \\ \dfrac{P_A}{ICI_A[K/2]+\sigma^2}, & \text{for } \delta_A \geq |\delta_B| \\ \dfrac{P_B}{ICI_B[K/2-1]+\sigma^2}, & \text{for } \delta_B \leq -|\delta_A| \\ \dfrac{P_A}{ICI_A[K/2-1]+\sigma^2}, & \text{for } \delta_A \leq -|\delta_B| \end{cases} \tag{20}$$

Hence, similar to $SINR_{pnc}^*$, $SINR_{ts}^*$ appears at subcarrier $\frac{K-1}{2}$ for an odd K, and depends on both δ_A and δ_B for an even K.

C. SINR Comparison

We are now in the position to compare the worst SINR in PNC with that in TS for $-0.5 < \delta_A, \delta_B < 0.5$. We find that $\frac{1}{2}SINR_{ts}^* < SINR_{pnc}^* \leq SINR_{ts}^*$ always holds in all situations, indicating that there is at most 3 dB SINR penalty in PNC relative to TS.

For an odd K: First, we compare $SINR_{pnc}^*$ with $SINR_{ts}^*$ when $|\delta_A| \geq |\delta_B|$. As mentioned in *Case 1 in TS* above, $ICI_i[\frac{K-1}{2}]$ increases as $|\delta_i|$ increases. Hence, we have $ICI_A[\frac{K-1}{2}] \geq ICI_B[\frac{K-1}{2}]$ for $|\delta_A| \geq |\delta_B|$ and thus $ICI_{pnc}[\frac{K-1}{2}]+\sigma^2 = ICI_A[\frac{K-1}{2}]+ICI_B[\frac{K-1}{2}]+\sigma^2 < 2\cdot(ICI_A[\frac{K-1}{2}]+\sigma^2)$. Eventually, for $|\delta_A| \geq |\delta_B|$, comparing (16) with (19), we get $\frac{1}{2}SINR_{ts}^* < SINR_{pnc}^* \leq SINR_{ts}^*$. Second, for $|\delta_A| < |\delta_B|$, it can be seen that the situation is similar to that of $|\delta_A| \geq |\delta_B|$ and the 3 dB bound of the SINR penalty in PNC still holds.

For an even K: We first compare $SINR_{pnc}^*$ with $SINR_{ts}^*$ in region 1 (i.e., $\delta_B \geq |\delta_A|$) in Fig. 11. As mentioned in *Case 2 in TS* above, in region 1, we must have $ICI_B[\frac{K}{2}] \geq ICI_A[\frac{K}{2}]$, and thus $ICI_{pnc}[\frac{K}{2}]+\sigma^2 = ICI_B[\frac{K}{2}]+ICI_A[\frac{K}{2}]+\sigma^2 < 2\cdot(ICI_B[\frac{K}{2}]+\sigma^2)$. As a result, for $\delta_B \geq |\delta_A|$, comparing (17) with (20), we get $\frac{1}{2}SINR_{ts}^* < SINR_{pnc}^* \leq SINR_{ts}^*$. In fact, by the same token, we find that the 3 dB bound of the SINR penalty in PNC also holds in the other three regions in Fig. 11.

To verify our analysis above, we compare $SINR_{pnc}^*$ with $SINR_{ts}^*$ in 802.11p VANETs (where K is an even number, $= 64$) for $-0.5 < \delta_A, \delta_B < 0.5$.

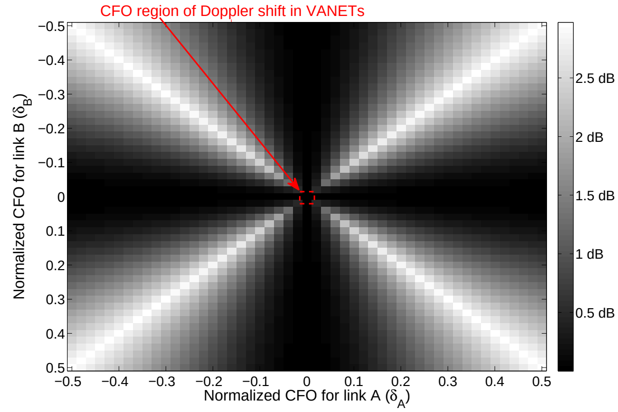

(a) SINR penalty (in dB) in PNC relative to TS

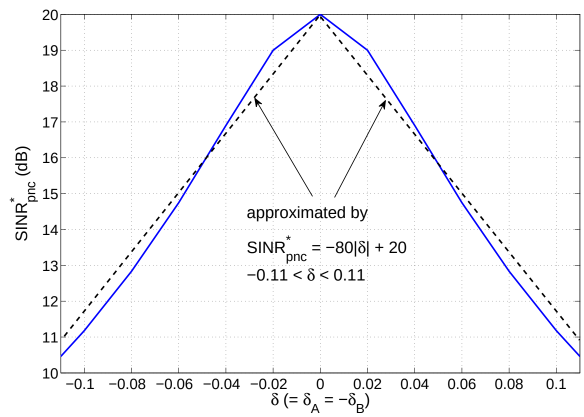

(b) $SINR_{pnc}^*$ over $-0.11 \leq \delta \leq 0.11$.

Fig. 2. SINR penalty and $SINR_{pnc}^*$ values at different (δ_A,δ_B) when $K = 64$ (SNR = 20 dB).

First, we verify (17) and (20). Given a (δ_A, δ_B) and a σ, we calculate $SINR_{pnc}[m]$ in (14) and $SINR_i[m]$ in (18) for all m and i, and then we compare the lowest $SINR_{pnc}[m]$ with $SINR_{pnc}^*$ in (17) and the lowest $SINR_i[m]$ with $SINR_{ts}^*$ in (20). Our numerical results (not shown as a figure here) show that for any (δ_A, δ_B), the lowest $SINR_{pnc}[m]$ and $SINR_i[m]$ are consistent with (17) and (20), respectively.

Next, we plot in Fig. 2(a) the SINR penalty in PNC relative to TS for SNR $= 20$ dB. First, we see from the color bar that at all values of (δ_A, δ_B), the SINR penalty in PNC is always within 3 dB. In fact, the SINR penalty at a larger σ becomes smaller. Second, we observe that a higher SINR penalty appears at (δ_A, δ_B) along the two diagonals (but not close to the origin). This is because $SINR_{pnc}^*$ approaches $\frac{1}{2}\cdot SINR_{ts}^*$ when $|\delta_A| = |\delta_B| > 0$. Third, a lower SINR penalty appears at (δ_A, δ_B) along the two axes, because $SINR_{pnc}^*$ approaches $SINR_{ts}^*$ when either $\delta_A \approx 0$ or $\delta_B \approx 0$. Hence, for low $|\delta_i| < 0.05$ in MANETs, e.g., when $f_{c,i}$ is synchronized with $f_{c,R}$ and $f_{d,i}$ contributes most to δ_i in VANETs (see the red rectangle in Fig. 2(a)), the SINR penalty in PNC is very limited.

Here we take a close look at how the SINR penalty will affect PNC in 802.11p VANET, as it is a standardized MANET. In 802.11p, due to low $f_{d,i}$, we simply assume

TABLE I
$\mathrm{E}(SINR^*_{pnc})$ VALUES AND SINR REQUIREMENTS FOR THE DATA RATES OF 802.11 TRANSMISSION

κ (ppm)	3.0	2.5	2.0	1.5	1.0	0.5
$\mathrm{E}(SINR^*_{pnc})$ (dB)	17.0	17.5	18.0	18.5	19.0	19.5
802.11a (Mbps)	24	-	-	-	36	-
802.11p (Mbps)	12	-	-	-	18	-
required SINR	17.0	-	-	-	18.8	-

$f_{\delta_i} = f_{o,i} - f_{o,R}$. Suppose $f_{o,i}$ and $f_{o,R}$ are uniformly distributed over $[f_c - \kappa f_c, f_c + \kappa f_c]$, where $f_c = 5.9$ GHz is the center frequency and κ denotes LO instability (in ppm). Section VI will introduce a CFO compensation which always yields $\delta_A = -\delta_B = \delta = \frac{f_{o,A}-f_{o,B}}{2\Delta_f}$. Thus, we are interested in $\mathrm{E}(SINR^*_{pnc})$ over δ. We use a linear function of δ (see Fig. 2(b) for SNR = 20 dB) to approximate $SINR^*_{pnc}$ over $-0.11 \le \delta \le 0.11$ (i.e., for $\kappa \le 3$ ppm), easing the estimation of $\mathrm{E}(SINR^*_{pnc})$. Table I shows $\mathrm{E}(SINR^*_{pnc})$ for different κ and the minimum SINR requirements for various data rates for 802.11 point-to-point transmission in TS [31]. We see that for $\kappa \le 3$ ppm, $\mathrm{E}(SINR^*_{pnc}) \ge 17$ dB holds. This is comparable with $SINR^*_{ts} = 20$ dB in the perfect case (with CFO eliminated in TS). It is not a surprise that PNC can support 12 Mbps or even higher per-link data rates in VANETs, given that the BER of PNC does not lag behind TS too much (this is actually the case as will be seen in Section VI).

V. IMPACT OF CFO ON BER OF PNC

This section explores signal detection schemes at relay R to mitigate the CFO/ICI effect on the bit error rate (BER) of PNC. We propose to use a belief propagation (BP) algorithm to tackle the ICI in PNC for relatively high CFO levels. Our study in this section focuses on PNC in the flat fading channel with no CFO compensation, and assumes ϕ_i and δ_i in (11) are known to relay R through channel estimation [10]. The case for the frequency-selective channel and with CFO compensation is considered in the next section.

A. Signal Detection in PNC

We need to deal with the ICI for the signal detection in PNC based on (11). Traditionally, the overall ICI in (11) is simply treated as Gaussian noise [10], [7], [32], with mean 0 and variance $ICI_{pnc}[m]$. In PNC, relay R aims to deduce $s_R[m] = s_A[m] \oplus s_B[m]$ from $y_R[m]$, and similar to the XOR-CD detector in [8], it takes the following two steps to get an estimate, $\widehat{s}_R[m]$, of $s_R[m]$ (Hereafter, we use the following short notations: $s_i^m = s_i[m]$, $y_R^m = y_R[m]$, and $\widehat{s}_R^m = \widehat{s}_R[m]$). First, relay R calculates the *a posteriori* probability $Pr((s_A^m, s_B^m)|y_R^m) \propto \exp\{-\left|y_R^m - \sum_{i\in\{A,B\}} e^{j\phi_i} a_{0,i} s_i^m\right|^2 \Big/ (\sigma^2 + ICI_{pnc}[m])\}$. Second, the maximum a posteriori probability (MAP) rule is used as follows to obtain the estimate $\widehat{s}_R^m$

$$\widehat{s}_R^m = \underset{s\in\{+1,-1\}}{\arg\max} \sum_{(s_A^m, s_B^m): s_A^m \oplus s_B^m = s} Pr((s_A^m, s_B^m)|y_R^m) \quad (21)$$

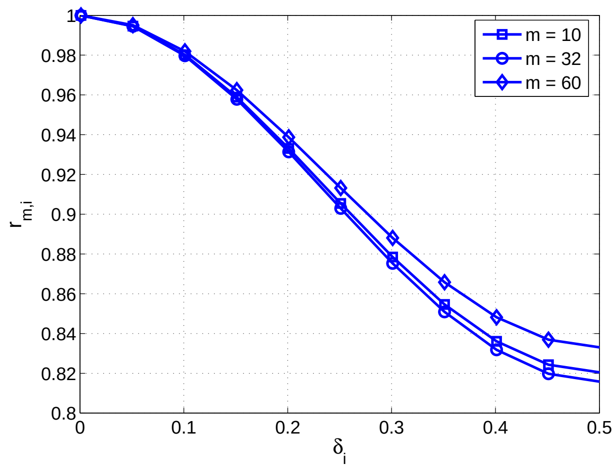

Fig. 3. Several examples of $r_{m,i}(\delta_i)$ in case of $K = 64$, $i \in \{A, B\}$ and $0 < m \le 63$.

This traditional detection scheme is called PNC with Gaussian interference (GI-PNC) in our paper, and will be used as the benchmark.

In GI-PNC, the detection of s_R^m is solely based on y_R^m in (11). In fact, (11) shows that for any m, s_A^m and s_B^m are involved in all the correlator outputs, hence a better scheme for s_R^m detection is to look at all y_R^m, $0 \le m \le K-1$. Equivalently, we now want to find $Pr((s_A^m, s_B^m)|(y_R^0, \ldots, y_R^{K-1}))$ (or $Pr(s_A^m, s_B^m)$ for simplicity) for any m. We propose a detection scheme called BP-PNC that uses BP to compute $Pr(s_A^m, s_B^m)$ and hence $\widehat{s}_R^m$. $Pr(s_A^m, s_B^m) \forall m$ is computed from $Pr((s_A^0, ..., s_A^{K-1}, s_B^0, ..., s_B^{K-1})|y_R^m \forall m)$, and the computation can be facilitated by BP based on the factorization of $Pr((s_A^0, ..., s_A^{K-1}, s_B^0, ..., s_B^{K-1})|y_R^m \forall m)$ (e.g., see (22) below). BP is a powerful tool for inference problems where a conditional marginal probability distribution like $Pr(s_A^m, s_B^m)$ is to be computed. For simplicity, our paper will focus on the procedures of BP. Interested readers are referred to [14], [15] for more details of BP.

Before delving into BP-PNC, we present a component analysis of y_i^m in (9). We find that for $\delta_i < 0$ ($\delta_i > 0$), the power of y_i^m excluding the noise is dominated by the desired subcarrier m and the adjacent interfering subcarrier $I_{m,i} = m + 1$ ($I_{m,i} = m - 1$). Defining $r_{m,i}(\delta_i) = (|a_{0,i}|^2 + |a_{1,i}|^2) \Big/ \sum_{u=m-K+1}^{m} |a_{u,i}|^2$ for $\delta_i > 0$, i.e., the ratio of the power from subcarriers m and $m-1$ over the total power of y_i^m, Fig. 3 plots $r_{m,i}(\delta_i)$ for different values of m when $K = 64$. We see from the figure that subcarriers m and $m-1$ together occupy most power of y_i^m, especially for not too high δ_i, e.g., $0 < \delta_i < 0.2$. In fact, for larger K, we find $r_{m,i}$ are essentially the same as in Fig. 3. Thus, relay R could deem that y_i^m in TS (y_R^m in PNC) is only composed of the desired signal plus the interference from subcarrier $I_{m,i}$ (subcarriers $I_{m,A}$ and $I_{m,B}$ of nodes A and B). With this simplified structure of y_R^m, BP-PNC considers the following four cases to detect s_R^m.

Case 1: $\delta_A > 0$ and $\delta_B > 0$. Here, we have $I_{m,A} =$

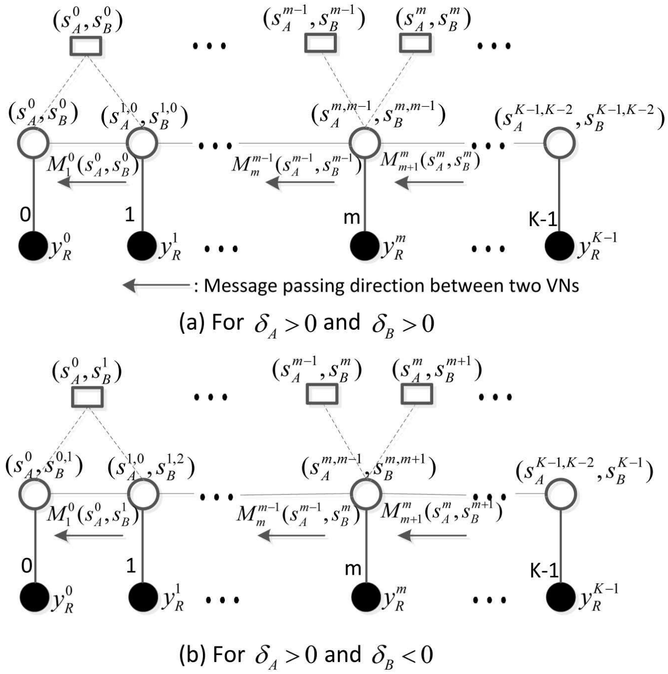

Fig. 4. Graphic Characterization of the correlation among the correlator outputs in PNC.

$I_{m,B} = m - 1$ for $m \neq 0$. For $m = 0$, all the interference in y_R^0 can simply be ignored, as it is very limited. Thus, a pairwise Markov random field (MRF) [15] can be used to characterize how the correlator outputs y_R^m are correlated, as shown in Fig. 4(a). In Fig. 4(a), the filled nodes are those observed correlator outputs y_R^m, and the empty circles are called variable nodes (VNs) representing the variables behind each observed y_R^m and to be inferred. In Fig. 4 and below, we use $s_i^{m,n} = (s_i^m, s_i^n)$. The variables behind y_R^1, for example, are the information bits $(s_A^{1,0}, s_B^{1,0})$. The edges between VNs represent their dependencies, and the square nodes show the common random variable(s) between them. In accordance with the MRF in Fig. 4(a), we have the following factorization:

$$
\begin{aligned}
&Pr((s_A^0, ..., s_A^{K-1}, s_B^0, ..., s_B^{K-1})|y_R^m \forall m) \\
&\propto Pr((s_A^0, s_B^0)|y_R^0) \prod_{m=1}^{K-1} Pr((s_A^{m,m-1}, s_B^{m,m-1})|y_R^m).
\end{aligned} \tag{22}
$$

Based on (22), BP-PNC takes the following steps to find $Pr(s_A^m, s_B^m)$ and $\widehat{s}_R^m$, for any m.

Step 1. Computing $Pr((s_A^{m,m-1}, s_B^{m,m-1})|y_R^m)$: This *a posteriori* probability is based on the local observation y_R^m only, and is computed as follows

$$
\begin{aligned}
&Pr((s_A^{m,m-1}, s_B^{m,m-1})|y_R^m) \\
&\propto \exp\{-\left|y_R^m - \sum\nolimits_i e^{j\phi_i}(a_{0,i}s_i^m + a_{1,i}s_i^{m-1})\right|^2 \Big/ \sigma^2\}
\end{aligned} \tag{23}
$$

Note that for $m = 0$, $Pr((s_A^0, s_B^0)|y_R^0)$ needs to be computed.

Step 2. Computing $Pr(s_A^m, s_B^m)$ using BP: To compute $Pr(s_A^m, s_B^m)$, BP takes the probability distributions in (23) as the input and applies message passing and updating between VNs in Fig. 4(a). BP first defines two messages between any two connected VNs: in Fig. 4(a), the two messages between the j-th and $j+1$-th VNs are denoted by $M_j^{j+1}(s_A^j, s_B^j)$ and $M_{j+1}^j(s_A^j, s_B^j)$, $0 \leq j \leq K-2$. Parts of the messages are displayed in Fig. 4(a). The message is used by one VN (specified in the subscript) to update the other (specified in the superscript) on the distribution of the common random variables (specified in the parenthesis). Once a VN receives an updated message from a neighbor node, it uses it to update the messages to other connected VNs.

The message update in Fig. 4(a) is performed in two directions, i.e., from the left to the right, and from the right to the left [14], [15], and the following equations state the message-update rules for $1 \leq j \leq K-2$.

$$
\begin{aligned}
&M_j^{j+1}(s_A^j, s_B^j) \\
&= \sum_{s_A^{j-1}} \sum_{s_B^{j-1}} \{Pr(s_A^{j,j-1}, s_B^{j,j-1}|y_R^j) M_{j-1}^j(s_A^{j-1}, s_B^{j-1})\}; \\
&M_j^{j-1}(s_A^{j-1}, s_B^{j-1}) \\
&= \sum_{s_A^j} \sum_{s_B^j} \{Pr(s_A^{j,j-1}, s_B^{j,j-1}|y_R^j) M_{j+1}^j(s_A^j, s_B^j)\}.
\end{aligned} \tag{24}
$$

The message update in the two directions starts at the two end VNs in Fig. 4(a), which update the following two messages

$$
\begin{aligned}
&M_0^1(s_A^0, s_B^0) = Pr(s_A^0, s_B^0|y_R^0); \\
&M_{K-1}^{K-2}(s_A^{K-2}, s_B^{K-2}) \\
&= \sum_{s_A^{K-1}} \sum_{s_B^{K-1}} Pr(s_A^{K-1,K-2}, s_B^{K-1,K-2}|y_R^{K-1}).
\end{aligned} \tag{25}
$$

Note that the probability distributions obtained in (23) keep fixed in the above message updating.

After the above message update in each direction is performed once, all the messages in Fig. 4(a) converge, thanks to the chain structure of the MRF in Fig. 4(a) [14]. Then, $Pr(s_A^m, s_B^m)$ is obtained at the m-th VN using all the received messages, i.e.,

$$
\begin{aligned}
Pr(s_A^m, s_B^m) \propto \sum_{s_A^{m-1}} \sum_{s_B^{m-1}} &\{Pr(s_A^{m,m-1}, s_B^{m,m-1}|y_R^m) \cdot \\
&M_{m-1}^m(s_A^{m-1}, s_B^{m-1}) \cdot M_{m+1}^m(s_A^m, s_B^m)\}.
\end{aligned} \tag{26}
$$

Note that for $m = 0$ and $m = K-1$, only one applicable message appears in (26).

Step 3. Determining $\widehat{s}_R^m$: Replacing $Pr((s_A^m, s_B^m)|y_R^m)$ in (21) with $Pr(s_A^m, s_B^m)$, $\widehat{s}_R^m$ is obtained.

Case 2: $\delta_A > 0$ and $\delta_B < 0$. Here, for $0 < m < K-1$, we have $I_{m,A} = m-1$ and $I_{m,B} = m+1$. For $m = 0$ ($m = K-1$), we have $I_{m,B} = 1$ ($I_{m,A} = K-2$) and the interference from all other subcarriers of node A (node B) are ignored in y_R^m. The MRF showing the correlation among all y_R^m in this case is plotted in Fig. 4(b). BP-PNC also conducts three steps to identify $\widehat{s}_R^m$. First, the *a posteriori* probabilities $Pr((s_A^{m,m-1}, s_B^{m,m+1})|y_R^m)$ are computed. Second, BP is applied to Fig. 4(b) to compute the desired $Pr(s_A^m, s_B^m)$. Third, based on $Pr(s_A^m, s_B^m)$, $\widehat{s}_R^m$ is determined using the MAP rule. These three steps are similar to those in ***Case 1***, hence the details are omitted.

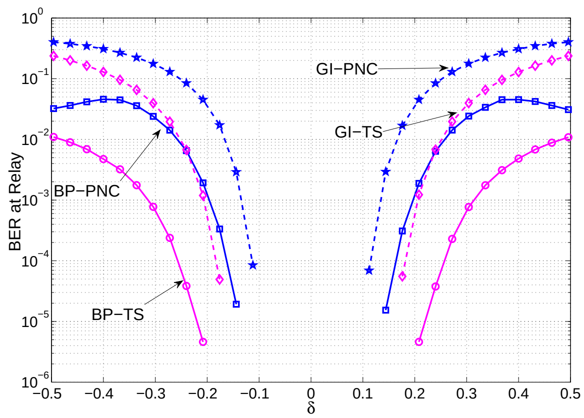

(a) $\phi_A = \phi_B = 0$ (i.e., $\Delta\theta = 0$)

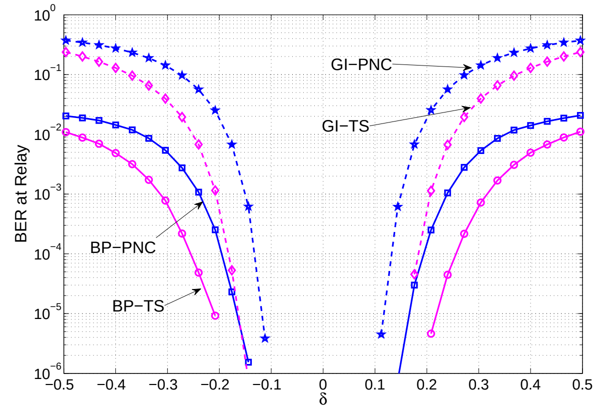

(b) $\phi_A = \frac{\pi}{4}$ and $\phi_B = 0$ (i.e., $\Delta\theta = \frac{\pi}{4}$)

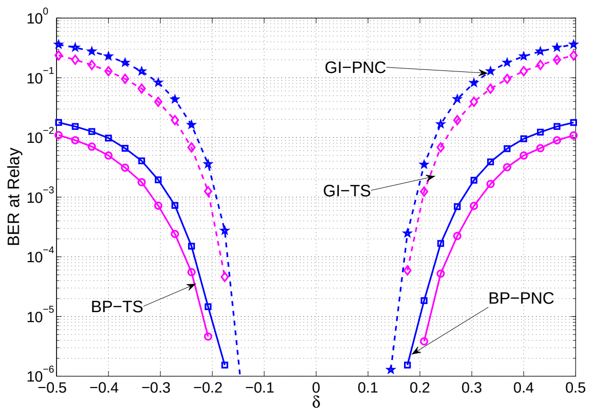

(c) $\phi_A = \frac{\pi}{2}$ and $\phi_B = 0$ (i.e., $\Delta\theta = \frac{\pi}{2}$)

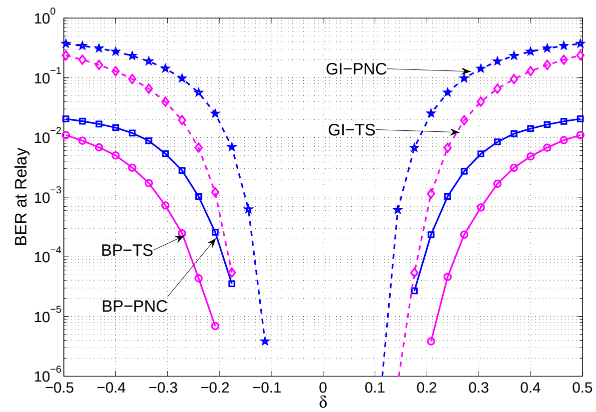

(d) $\phi_A = \frac{3\pi}{4}$ and $\phi_B = 0$ (i.e., $\Delta\theta = \frac{3\pi}{4}$)

Fig. 5. BER comparison at relay R at different δ and $\Delta\theta$ (SNR = 20 dB).

Case 3: $\delta_A < 0$ and $\delta_B < 0$. Here, the graph of the MRF is very similar to that in *Case 1*, and the details are omitted.

Case 4: $\delta_A < 0$ and $\delta_B > 0$. Here, the graph of the MRF is very similar to that in *Case 2*, and the details are omitted.

B. Signal Detection in TS

For a fair comparison, we also consider two signal detection schemes in TS at relay R. The first scheme is called GI-TS, which treats the ICI in (9) as Gaussian noise. Similar to GI-PNC, GI-TS first calculates $Pr(s_i^m|y_i^m)$, and then applies MAP rule to detect s_i^m. The second scheme is called BP-TS, which uses BP to compute $P(s_i^m|(y_i^0,\ldots,y_i^{K-1}))$ (or simply $P(s_i^m)$). $\delta_i > 0$ and $\delta_i < 0$ are the two cases in BP-TS, corresponding to two MRF graphs. The message passing and updating in the two graphs are similar to that in BP-PNC, and s_i^m is detected by applying the MAP rule to the distribution $P(s_i^m)$.

Remark: It can be seen that the four detection schemes above are not limited to BPSK. They can be readily applied to any other higher-order modulation, e.g., QPSK, considering all possible constellation points for s_i^m in that modulation.

C. Complexity Analysis

Now we analyze the complexity of BP-PNC. To be general, let N_m be the size of a modulation scheme used in BP-PNC, e.g., $N_m = 2$ for BPSK and $N_m = 4$ for QPSK. For ***Case 1***, as $K \to \infty$, the complexity of (23) is $O(K \cdot N_m^4)$; the complexity of message passing in (24) is $O(2 \cdot (K-1) \cdot N_m^4)$; and the complexity of the belief read-out in (26) is $O(K \cdot N_m^4)$. Thus, the overall complexity of BP-PNC is simply $O(K \cdot N_m^4)$. It is not difficult to see that this complexity applies to all other three cases. By the same token, we find that the complexity of BP-TS is $O(K \cdot N_m^2)$.

D. BER Performance Evaluation

Now we study the BER of BP-PNC at relay R under BPSK modulation, compared with GI-PNC, GI-TS, and BP-TS. [14], [20] showed that the BER of PNC at relay R was affected by the relative phase offset even without CFO in (11), and [5], [23] showed that it was also affected by the CFO. Here, we explicitly study the joint effect of the relative phase offset $\Delta\theta$ as defined in Section III-B and the CFO δ_i on the BER of PNC. Our study assumes $\delta_A = \delta_B = \delta$ and looks at the effect of the CFO δ at different given values of $\Delta\theta$ (here reduced to $\phi_A - \phi_B$). We consider a MANET with $K = 64$, $T_s = 6.4$ µs, and CP length equal to $\frac{T_s}{4}$, as adopted in 802.11p. Fig. 5 plots the simulation results, and the key observations are as follows.

First, as $|\delta|$ increases (or in a MANET with higher node mobility), the BER of the four schemes deteriorates for any $\Delta\theta$, but the scheme using BP in either PNC or TS is more robust against the CFO. A larger $|\delta|$ decreases the power of the desired signal in both (9) and (11), shortening the distances between the received constellation points in both TS and PNC. Thus, a higher $|\delta|$ yields higher BER for all the schemes. The reason for the robustness of BP-PNC and BP-TS is due to the certainty propagation in BP [14]. For BP-PNC with $\delta > 0$, for example, Fig. 4(a) shows that y_R^0 is less interfered than the others, thus enabling the detection of (s_A^0, s_B^0) with high confidence. With message passing in BP, this confidence of detection reduces uncertainties about y_R^1 and improves the detection of (s_A^1, s_B^1) (as reflected in (26)), which then further benefits the signal detection on other subcarriers. This is the certainty propagation, and it also applies to BP-TS and the other cases in BP-PNC.

Second, as $\Delta\theta$ increases from 0 to $\frac{\pi}{2}$, the BER of BP-PNC (GI-PNC) becomes lower and close to that of BP-TS (GI-TS). Here we focus on the reasons for BP-PNC. We find that a larger $\Delta\theta$ within $\left[0, \frac{\pi}{2}\right]$ helps isolate the received constellation points at relay R in BP-PNC. Consider $\delta = 0.2$ for example. Fig. 6 plots the received constellation diagram of $(s_A^{m,m-1}, s_B^{m,m-1})$ ($m \geq 1$) for different $\Delta\theta$. Each point in Fig. 6 conveys (i) a circle (square) shape denotes $s_A^m \oplus s_B^m = -1$ ($s_A^m \oplus s_B^m = +1$), and (ii) the number near it denotes the interference (s_A^{m-1}, s_B^{m-1}). We see from Fig. 6 that as $\Delta\theta$ increases, these points are more isolated, and in particular, the shortest distance between any two points having different $s_A^m \oplus s_B^m$ increases, thus improving the certainty of detecting $s_R^m = s_A^m \oplus s_B^m$ even without the certainty propagation in BP.

Third, the BER curve of BP-PNC at $\Delta\theta$ is the same as that at either $\pi + \Delta\theta$ or $\pi - \Delta\theta$. The reason is that the received constellation diagrams, e.g., for $(s_A^{m,m-1}, s_B^{m,m-1})$, in these three situations have the same pattern, e.g., the shortest distance mentioned above keeps the same. For example, the BER curve of BP-PNC at $\Delta\theta = \frac{3\pi}{4}$ (shown in Fig. 5(d)) is basically the same as that at $\Delta\theta = \frac{\pi}{4}$.

In fact, even for $\delta_A \neq \delta_B$, we observe that the following two properties are present in all the four cases of BP-PNC: (i) the received constellation points like $(s_A^{m,m-1}, s_B^{m,m-1})$ in ***Case 1*** are more isolated when $\Delta\theta = \frac{\pi}{2}$, and (ii) the constellation diagrams at $\pi \pm \Delta\theta$ keep the same pattern as that at $\Delta\theta$. Overall, our study here shows that despite CFO deteriorating the BER of BP-PNC, the relative phase offset $\Delta\theta$ close to $\pi \pm \frac{\pi}{2}$ can mitigate the CFO effect.

VI. CFO Compensation in PNC

This section studies CFO compensation in PNC, aiming to reduce the CFO effect on both the SINR and BER of PNC.

Using training symbols, the CFO of one link can be estimated [10]. With this estimated CFO, i.e., $\widetilde{f_{\delta_i}}$ ($= f_{\delta_i}$ for an accurate estimate), the effect of CFO in TS can be eliminated

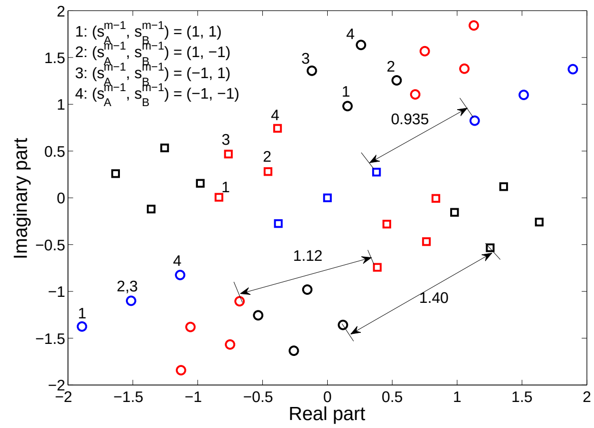

Fig. 6. Received constellation diagram of $(s_A^{m,m-1}, s_B^{m,m-1})$ at $\delta = 0.2$ for different $\Delta\theta$. Blue points: $\phi_A = \phi_B = 0$; red points: $\phi_A = \frac{\pi}{4}$, $\phi_B = 0$; black points: $\phi_A = \frac{\pi}{2}$, $\phi_B = 0$.

via signal processing, which is equivalent to adjusting relay R's LO frequency at the m-th correlator in (5) from f_m to $f_m + \widetilde{f_{\delta_i}}$ to match $f_m + f_{\delta_i}$ [10]. However, it is normally the case that the CFO values for the two uplinks in PNC are different, thus ruling out the possibility for relay R to match the frequencies $f_m + f_{\delta_A}$ and $f_m + f_{\delta_B}$ at the same time. Hence, in this situation, we seek an effective CFO compensation in PNC, and propose the mean-frequency (MF) compensation which amounts to positioning relay R's LO frequency at the middle of the received frequencies from the two end nodes, that is, the adjusted frequency $f_m^{'}$ is given by

$$f_m^{'} = f_m + \frac{f_{\delta_A} + f_{\delta_B}}{2}, \text{ for } 0 \leq m \leq K-1 \quad (27)$$

A. Effect of MF Compensation on SINR

We show below that this MF compensation, as stated by the following theorem, can yield a maximal $SINR_{pnc}^*$.

Theorem 1: Among CFO compensations that equivalently adjust relay R's LO frequency by $\tau \cdot \Delta_f$, where τ satisfies $|\delta_A - \tau| < 0.5$ and $|\delta_B - \tau| < 0.5$, the MF compensation maximizes $SINR_{pnc}^*$, i.e., $SINR_{pnc}^*$ achieves a (local) maximum at $\tau = \frac{\delta_A + \delta_B}{2}$.

Proof: Let us first consider the case when K is an odd number. As the phase term, $e^{j\phi_i}$ or $e^{j\phi_{m,i}}$, of the channel gain function is irrelevant to $SINR_{pnc}[m]$ defined in (14), we drop it in our proof below. Replacing f_m with $f_m + \tau \cdot \Delta_f$ in (5), the output of the m-th correlator at relay R is given by

$$y_R[m] = \sum_i a_{0,i}^{'} s_i[m] + \sum_{u \neq 0} \sum_i a_{u,i}^{'} s_i[m-u] + w_m \quad (28)$$

where u and w_m are defined the same as earlier, and $a_{u,i}^{'} = \frac{1}{T_s} \int_0^{T_s} e^{-j2\pi(u+\tau-\delta_i)t/T_s} dt$, for $i \in \{A, B\}$. Due to $|\delta_i - \tau| < 0.5$ for $i \in \{A, B\}$, the $\frac{K-1}{2}$-th subcarrier in PNC still has the worst SINR. Thus, we obtain

$$SINR^*_{pnc} = \frac{\min\{\mathrm{sinc}^2(\delta_A - \tau), \mathrm{sinc}^2(\delta_B - \tau)\}}{\sum\limits_{u=(1-K)/2, u\neq 0}^{(K-1)/2} \sum\limits_{i} \mathrm{sinc}^2(u - \delta_i + \tau) + \sigma^2} \quad (29)$$

Defining $\tau = \varepsilon + \frac{\delta_A+\delta_B}{2}$ and assuming $2d = \delta_B - \delta_A$, (29) becomes

$$SINR^*_{pnc}(\varepsilon) = \frac{\min\{\mathrm{sinc}^2(d-\varepsilon), \mathrm{sinc}^2(d+\varepsilon)\}}{\sum\limits_{u\neq 0}\{\mathrm{sinc}^2(u+\varepsilon-d) + \mathrm{sinc}^2(u+\varepsilon+d)\} + \sigma^2} \quad (30)$$

In (30), let $P(\varepsilon)$ denote the function at the numerator and $Q(\varepsilon)$ denote the function at the denominator. Then, it is not difficult to see that $P(\varepsilon)$ and $Q(\varepsilon)$ are *even* functions of ε, both continuous at $\varepsilon = 0$. Thus, $SINR^*_{pnc}(\varepsilon)$ must achieve a local extremum at $\varepsilon = 0$. We now examine the following two cases for $SINR^*_{pnc}(\varepsilon)$ at $\varepsilon = 0$.

Case 1: $\delta_A = \delta_B$. Here we have $d = 0$, $P(0) = \mathrm{sinc}^2(0)$, and $Q(0) = \sigma^2$. Obviously, at $\varepsilon = 0$, $P(\varepsilon)$ achieves a global maximum, whereas $Q(\varepsilon)$ achieves a global minimum. Therefore, $SINR^*_{pnc}(\varepsilon)$ achieves a global maximum at $\varepsilon = 0$.

Case 2: $\delta_A \neq \delta_B$. With $-0.5 < \delta_A, \delta_B < 0.5$, we have $-0.5 < d < 0.5$ and $d \neq 0$. For this range of d, it is not difficult to find that $P(\varepsilon = 0) = \mathrm{sinc}^2(d)$ is a local maximum, and that the left derivative and the right derivative of $P(\varepsilon)$ at $\varepsilon = 0$ are equal to $\frac{dy}{dx}|_{x=-d}$ and $\frac{dy}{dx}|_{x=d}$ where $y = \mathrm{sinc}^2(x)$, respectively; these two derivatives are both non-zero and opposite to each other. By contrast, we have $\frac{dQ}{d\varepsilon}|_{\varepsilon=0} = 0$, both the left and the right derivatives equal to 0. This means for ε around 0, $P(\varepsilon)$ decreases drastically from $P(\varepsilon = 0)$ whereas $Q(\varepsilon)$ stays almost constant. In this situation, $SINR^*_{pnc}(\varepsilon = 0)$ hence achieves a local maximum.

Combining the two cases above, we see that $SINR^*_{pnc}$ achieves a maximum at $\varepsilon = 0$ or at $\tau = \frac{\delta_A+\delta_B}{2}$ equivalently.

For an even K, we note that $SINR^*_{pnc}(\varepsilon)$ is also an even function, and thus the proof is similar to that for an odd K. Details are omitted here for simplicity. ∎

Fig. 7 shows $SINR^*_{pnc}$ (not in dB) in two belt regions of (δ_A, δ_B) when $K = 64$, and briefly illustrates the effect of the MF compensation in achieving a maximal $SINR^*_{pnc}$. Suppose the CFO for the two uplinks in PNC are δ^0_A and δ^0_B, respectively. Then, after the LO adjustment is applied with a certain τ, it is equivalent that (δ^0_A, δ^0_B) becomes $(\delta^0_A - \tau, \delta^0_B - \tau)$. Thus, with different τ, (δ^0_A, δ^0_B) moves along the line $\delta_B = \delta_A + 2d$ in Fig. 7, where $2d = \delta^0_B - \delta^0_A$. It can be seen from Fig. 7 that (i) when (δ^0_A, δ^0_B) moves to the joint point between $\delta_B = \delta_A + 2d$ and $\delta_B = -\delta_A$, a maximal $SINR^*_{pnc}$ is achieved, and (ii) at the joint point we have $\tau = \frac{\delta^0_A+\delta^0_B}{2}$, which is consistent with that in the MF compensation. In addition, Fig. 7 also shows that the maximal $SINR^*_{pnc}$ only depends on d and it decreases as $|d|$ increases.

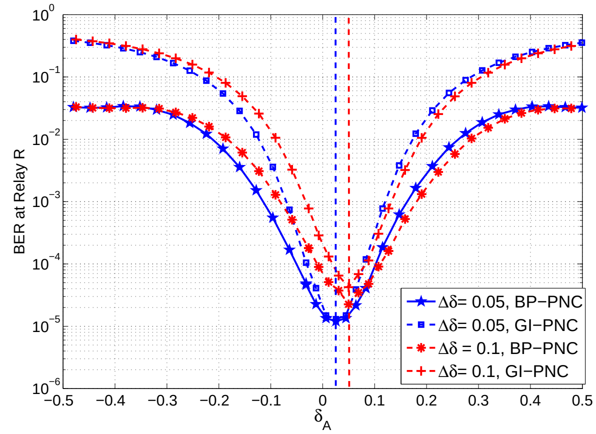

Fig. 8. Effect of MF compensation on the BER of BP-PNC and GI-PNC ($\phi_A = \phi_B = 0$ and SNR = 10 dB).

B. Effect of MF compensation on BER

We now study the effect of the MF compensation on the BER of PNC. We continue adopting the simulation setting in Section V-D. Our study below considers each end node sending a long packet composed of $L = 150$ OFDM symbols and assumes flat fading channels in TWRC. We look at the BER averaged over all the OFDM symbols.

First, we examine if the MF compensation could also be BER-optimal given a $\Delta\delta$ (defined as $|\delta_A - \delta_B|$). For a given $\Delta\delta$, we assume $\delta_A - \delta_B = \Delta\delta$ and plot in Fig. 8 the BER of BP-PNC and GI-PNC at relay R at different (δ_A, δ_B). We see from Fig. 8 that for any $\Delta\delta$, both BP-PNC and GI-PNC attain optimal BER at $(\delta_A, \delta_B) = (\frac{\Delta\delta}{2}, -\frac{\Delta\delta}{2})$, indicating that with the MF compensation in either BP-PNC or GI-PNC, an optimal BER at relay R could be obtained. Moreover, we find that the results in Fig. 8 keep unchanged for any ϕ_A and ϕ_B. We focus on the reasons for BP-PNC. (6) shows that CFO has a rotating effect on OFDM symbols, i.e., every OFDM symbol is rotated by $2\pi f_{\delta_i} T$ more than its previous symbol in a packet, where T is the overall length of an OFDM symbol including the CP. Thus, when $\delta_A \neq \delta_B$, it is most likely that different OFDM symbols in a packet undergo different $\Delta\theta$, with $\Delta\theta$ evenly distributed over $[0, 2\pi]$ regardless of ϕ_A or ϕ_B. As discussed in Section V-D, these symbols then experience different constellation diagrams (some are good, some are bad), which keeps the average BER in Fig. 8 not affected by ϕ_A or ϕ_B.

Second, for a fixed $\Delta\delta \neq 0$, we study the BER of BP-PNC and GI-PNC at different (δ_A, δ_B) when the MF compensation is applied. Our simulation results (not shown as a figure here) show that the BER of both schemes depends only on $\Delta\delta$.

Next, we compare BP-PNC and GI-PNC (both with the MF compensation) at different $\Delta\delta$ and SNR levels, as plotted in Fig. 9. We include the BER of TS with CFO eliminated as a reference. Note that without CFO, BP-TS and GI-TS have the same BER. Fig. 9 shows that (i) at low $\Delta\delta \leq 0.05$, both BP-PNC and GI-PNC achieve a BER close to that of TS, and (ii) as $\Delta\delta$ increases, BP-PNC outperforms GI-PNC. Fig. 9 also shows that to achieve a BER on the order of 10^{-6}, BP-PNC

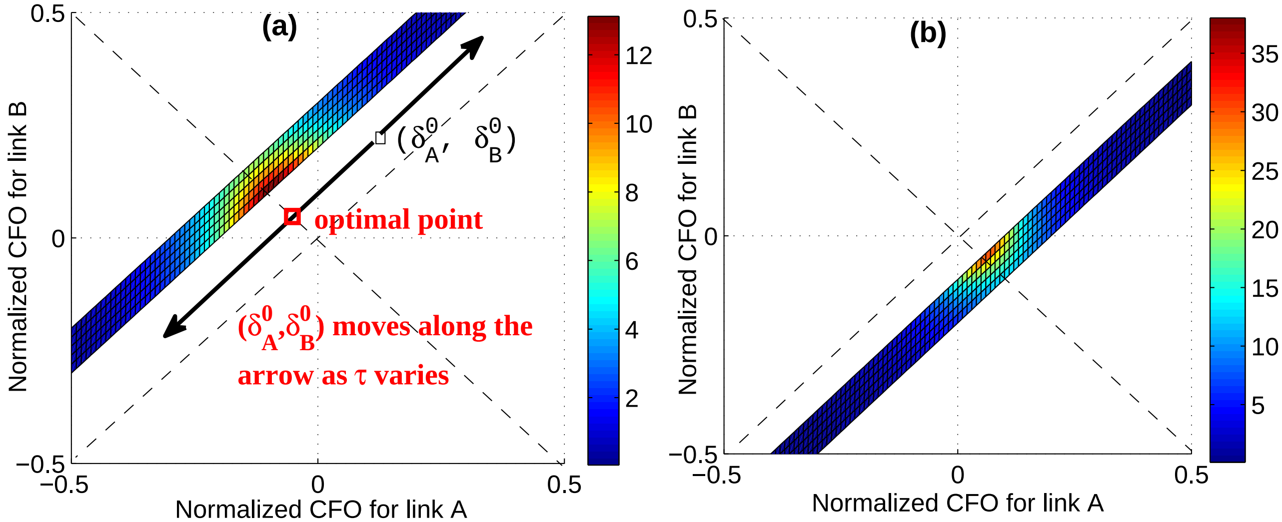

Fig. 7. Illustration of MF compensation for achieving a maximal $SINR^*_{pnc}$ (SNR = 20 dB). (a): $0.2 \leq 2d \leq 0.3$. (b): $-0.2 \leq 2d \leq -0.1$

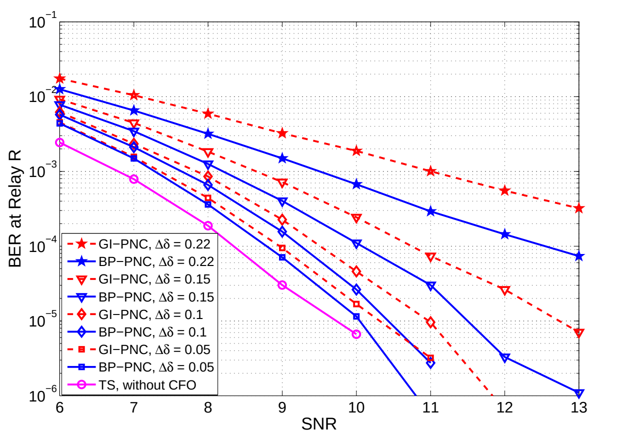

Fig. 9. BER comparison of BP-PNC and GI-PNC under MF compensation ($\phi_A = \phi_B = 0$).

needs at most 3 dB extra SNR compared with TS, for not too high $\Delta\delta \leq 0.15$. Note that this 3 dB extra SNR can be traded for halved transmission times in TWRC, as the downlink BER of PNC is generally comparable to that of TS [16].

We also consider the performance of BP-PNC and GI-PNC in frequency-selective TWRC, and compare them at different $\Delta\delta$ and SNR levels. Here, BP-PNC and GI-PNC are similarly designed as in the flat fading channel. We find that the BER curves are nearly the same as those in Fig. 9 and are not affected by $\phi_{m,i}$, for all i and m. The reason is similar to that in flat-fading TWRC above, that is, the rotating effect of the CFO on OFDM symbols in a packet corresponds to an averaging effect on the BER of BP-PNC over a packet in general, regardless of $\phi_{m,i}$.

Going beyond the studies above that assume the CFO δ_i is perfectly known to relay R, we now study the effect of CFO estimation error e_i on BP-PNC. Applying the MF compensation at relay R, the estimated CFO for node A (B) becomes $\frac{\delta_A-\delta_B+e_A-e_B}{2}$ $(-\frac{\delta_A-\delta_B+e_A-e_B}{2})$, whereas the actual CFO value becomes $\frac{\delta_A-\delta_B}{2} - \frac{e_A+e_B}{2}$ $(\frac{\delta_B-\delta_A}{2} - \frac{e_A+e_B}{2})$, indicating a deviation of e_A (e_B) between the estimated and actual CFO values. Similar to [19], we assume e_i is Gaussian distributed with zero mean and variance σ_e^2.

For different $\Delta\delta = |\delta_A - \delta_B|$ and packet length L, Fig. 10 plots the effect of e_A and e_B when σ_e is fixed at 6×10^{-3} (yielding $\mathrm{E}(|e_i|) \approx 5 \times 10^{-3}$). First, for both $\Delta\delta = 0.1$ and $\Delta\delta = 0.15$, the BER at relay R deteriorates as L increases. The reason is as follows. At relay R with $e_i \neq 0$, there is a phase estimation error for the signal from node i, and particularly, this error accumulates from one OFDM symbol to the next. The average accumulation rate in our simulation setting is $2\pi \cdot \mathrm{E}(|e_i|) \cdot \Delta_f \cdot (T_s + \frac{T_s}{4})$ rad $\approx 2.25°$. Thus, as L increases, the BER of BP-PNC is degraded. Second, the curves for $L = 10$ and $L = 15$ show that the accumulation of the phase estimation error is rather harmful and dominates the BER performance of BP-PNC, regardless of $\Delta\delta$ and the SNR values. This indicates the significance of maintaining a low phase estimation error (e.g., using pilots) in BP-PNC.

VII. Conclusion

This paper has addressed an outstanding issue on the feasibility of PNC in a two-way relay channel (TWRC) in MANETs: how to mitigate the CFO/ICI effects in PNC systems caused by node-motion induced Doppler shifts and/or the local oscillator (LO) asynchrony.

We have studied the effect of CFO on the SINR in PNC. We compare the worst SINR among all the subcarriers at the relay in PNC with that in TS. With a practical power control that balances the power levels of the received signals at the relay, our studies show that PNC suffers at most 3 dB SINR penalty in either the flat fading channel or the frequency-selective channel. A high SINR penalty arises when $|\delta_A| = |\delta_B| > 0$ and a low SINR penalty arises when either $\delta_A \approx 0$ or $\delta_B \approx 0$,

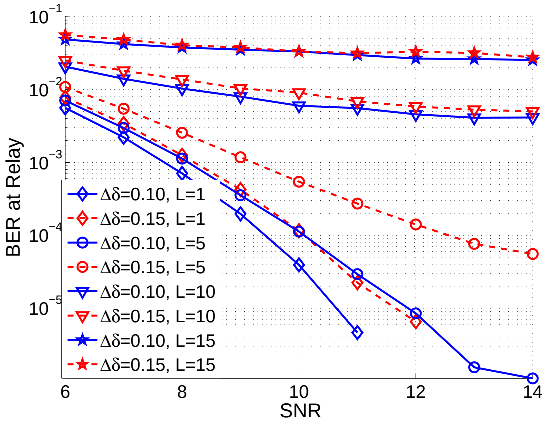

Fig. 10. The effect of the CFO estimation errors on BP-PNC ($\sigma_e = 6 \times 10^{-3}$).

where δ_i, $i \in \{A, B\}$, is the normalized CFO of the uplink from node i to the relay in TWRC.

We have also studied the effect of CFO on the BER of PNC at the relay, with two detectors considered. GI-PNC is a traditional detector that treats the ICI as Gaussian noise, and BP-PNC is a detector proposed by us with an attempt to effectively reduce the CFO effect. BP-PNC exploits the correlation among the OFDM correlator outputs and makes use of a belief propagation (BP) algorithm for signal detection. As an important result, our studies in flat fading channels based on BPSK modulation show that CFO is detrimental to the BER of BP-PNC and GI-PNC, but interestingly, a relative phase offset close to $\pi \pm \frac{\pi}{2}$ between the desired signals from the end nodes could mitigate the CFO negative effect.

To further mitigate the CFO effect in PNC, we have proposed a CFO compensation method called the mean-frequency (MF) compensation to equivalently position the relay's LO frequency at the middle of the received frequencies from the two end nodes. We show that this MF compensation can maximize the worst SINR in PNC and minimize the BER of BP-PNC and GI-PNC under BPSK modulation, regardless of the channel gain functions in TWRC. Importantly, with the MF compensation, we show that for low $|\delta_A - \delta_B| < 0.05$, GI-PNC is a suitable detector at the relay to attain a BER close to that in the ideal case, i.e., TS without CFO. For a higher $|\delta_A - \delta_B| \leq 0.15$, BP-PNC is a better choice that needs only at most 3 dB extra SNR to be comparable with the ideal case. Overall, for BPSK modulated MANETs with low to medium CFO levels ($|\delta_A - \delta_B| \leq 0.15$), PNC system works fine in principle as a performance booster.

For future work, we aim to (1) integrate channel coding to improve BP-PNC, and (2) to extend BP-PNC to higher-order modulations such as QPSK. Especially, for (2), despite the fact that BP-PNC can be readily applied to higher-order modulations, the challenge is that the XOR decoding situation therein will be more complicated under CFO and phase asynchrony, according to [14]. In addition to (1) and (2), exploiting pilots to combat the accumulation of the phase estimation error in the uplink transmission of PNC is of significant importance.

Appendix A

Here, we first determine the subcarrier(s) in TS that suffers from the maximal ICI power under FPC. Consider $d_i(m) = ICI_i[m] - ICI_i[m-1]$, for $1 \leq m \leq K-1$ and $i \in \{A, B\}$. Due to $ICI_i[m] = \sum_{u \neq 0} \mathrm{sinc}^2(u - \delta_i)$, we have $d_i(m) = \mathrm{sinc}^2(m - \delta_i) - \mathrm{sinc}^2(K - m + \delta_i)$.

Case 1 in TS: for an odd $K \geq 3$. If $m < \frac{K-1}{2}$, we have $K - m > \frac{K+1}{2}$. It is not difficult to see that for $|\delta_i| < 0.5$, the function $h(\delta_i) = \mathrm{sinc}^2(u_1 - \delta_i) - \mathrm{sinc}^2(u_2 + \delta_i) > 0$ always holds, when $u_1 < u_2$ and both are positive integers. Hence, considering $m < \frac{K-1}{2}$ and $K - m > \frac{K+1}{2}$, we have $d_i(m) > 0$ for $|\delta_i| < 0.5$. If $m = \frac{K-1}{2}$, we have $K - m = \frac{K+1}{2}$, yielding $d_i(m) > 0$. If $m > \frac{K-1}{2}$, we have $K - m < \frac{K+1}{2}$, yielding $d_i(m) < 0$. Therefore, for an odd K and $|\delta_i| < 0.5$, the $\frac{K-1}{2}$-th subcarrier or the middle subcarrier suffers from the maximal ICI power.

Case 2 in TS: for an even $K \geq 2$. Similar to *Case 1* above, here we have $d_i(m) > 0$ for $m < \frac{K}{2}$ and $d_i(m) < 0$ for $m > \frac{K}{2}$. For $m = \frac{K}{2}$, we have $d_i(\frac{K}{2}) = \mathrm{sinc}^2(\frac{K}{2} - \delta_i) - \mathrm{sinc}^2(\frac{K}{2} + \delta_i)$. Obviously, we have $d_i(\frac{K}{2}) \geq 0$ for $0 \leq \delta_i < 0.5$ and $d_i(\frac{K}{2}) < 0$ for $-0.5 < \delta_i < 0$. Therefore, for an even K, when $0 \leq \delta_i < 0.5$, it is the $\frac{K}{2}$-th subcarrier that suffers from the maximal ICI power; otherwise, it is the $\frac{K-2}{2}$-th subcarrier.

In PNC, we have $ICI_{pnc}[m] = ICI_A[m] + ICI_B[m]$. Thus, for an odd K, $ICI_{pnc}[\frac{K-1}{2}]$ must be the largest among all $ICI_{pnc}[m]$; and for an even K in PNC, the largest ICI power must be present at either the $\frac{K}{2}$-th subcarrier or the $\frac{K-2}{2}$-th subcarrier.

Appendix B

For an even K in TS , we know from Appendix A that the largest $ICI_i[m]$ for all i and m can only be $ICI_A[\frac{K}{2}]$, $ICI_A[\frac{K-2}{2}]$, $ICI_B[\frac{K}{2}]$, or $ICI_B[\frac{K-2}{2}]$. The conditions for $ICI_A[\frac{K}{2}]$ to be the largest are as follows. First, we must have $\delta_A \geq 0$. Second, if $\delta_B \geq 0$, we must have $\delta_A \geq \delta_B$ to have $ICI_A[\frac{K}{2}] \geq ICI_B[\frac{K}{2}]$. This is because we observe that $ICI_i[\frac{K}{2}]$ is increasing as δ_i increases from 0 to 0.5. If $\delta_B < 0$, we must have $\delta_A \geq -\delta_B$ to have $ICI_A[\frac{K}{2}] \geq ICI_B[\frac{K-2}{2}]$. This is because it can be further observed that $ICI_B[\frac{K-2}{2}]$ is increasing as δ_B decreases from 0 to -0.5, and that $ICI_B[\frac{K-2}{2}] = ICI_A[\frac{K}{2}]$ when $\delta_B = -\delta_A$. The conditions for $ICI_A[\frac{K-2}{2}]$, $ICI_B[\frac{K}{2}]$, or $ICI_B[\frac{K-2}{2}]$ to be the largest can be similarly obtained; we summarize them in Fig. 11.

For an even K in PNC, we know that the largest $ICI_{pnc}[m]$ arises at either $m = \frac{K}{2}$ or $m = \frac{K-2}{2}$. As defined in Appendix A, we have $d_i(\frac{K}{2}) = \mathrm{sinc}^2(\frac{K}{2} - \delta_i) - \mathrm{sinc}^2(\frac{K}{2} + \delta_i)$, which is an odd function of δ_i and is increasing as δ_i increases from 0 to 0.5. Thus, we have $ICI_{pnc}[\frac{K}{2}] \geq ICI_{pnc}[\frac{K-2}{2}]$ when $\delta_A \geq |\delta_B|$ or $\delta_B \geq |\delta_A|$; and we have $ICI_{pnc}[\frac{K}{2}] \leq ICI_{pnc}[\frac{K-2}{2}]$ when $\delta_A \leq -|\delta_B|$ or $\delta_B \leq -|\delta_A|$. Fig. 11 summarizes the conditions for $ICI_{pnc}[\frac{K}{2}]$ or $ICI_{pnc}[\frac{K-2}{2}]$ to be the largest.

References

[1] F. Li and Y. Wang, "Routing in vehicular ad hoc networks: a survey," *IEEE Vehicular Technology Magazine*, vol. 2, no. 2, pp. 12 - 22, 2007.

[2] R. Coutinho, A. Boukerche, L. Vieira, and A. Loureiro, "Design guidelines for opportunistic routing in underwater networks," in *IEEE Communications Magazine*, vol. 54, no. 2, pp. 40 - 48, 2016.

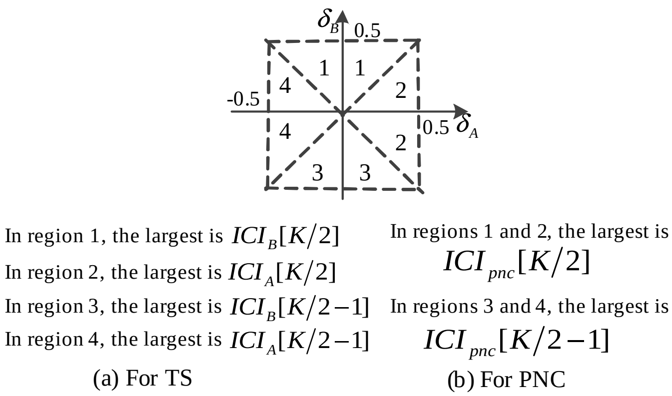

Fig. 11. The largest $ICI_i[m]$ and $ICI_{pnc}[m]$ in different regions of (δ_A, δ_B) for an even K.

[3] I. W.-H. Ho, R. North, J. Polak, and K. Leung, "Effect of transport models on connectivity in inter-bus communication networks," *Journal of ITS*, vol. 15, no. 3, pp. 161 - 178, 2011.

[4] "IEEE Std. 802.11p-2010, Part 11: Wireless LAN MAC and PHY Specifications Amendment 6 - Wireless Access in Vehicular Environments," IEEE Std. 802.11, 2010.

[5] Z. Wang, J. Huang, S. Zhou, and Z. Wang, "Iterative receiver processing for OFDM modulated physical-layer network coding in underwater acoustic channels," *IEEE Trans. Commun.*, vol. 61, no. 2, pp. 541 - 553, 2013.

[6] S. Zhang, S. C. Liew, and P. P. Lam, "Physical-layer network coding," in *Proc. of MobiCom*, 2006.

[7] A. Ligata, H. Gacanin, and F. Adachi, "On performance of analog network coding in the presence of phase noise," *EURASIP Journal on Wireless Communications and Networking*, 2013.

[8] S. C. Liew, S. Zhang, and L. Lu, "Physical-layer network coding: tutorial, survey, and beyond," *Physical Communication*, vol. 6, pp. 4 - 42, 2013.

[9] T. Wang, J. Proakis, E. Masry, and J. Zeidler, "Performance degradation of OFDM systems due to Doppler spreading," *IEEE Trans. Wireless Commun.*, vol. 5, no. 6, 2006.

[10] L. Lu, T. Wang, S. C. Liew, and S. Zhang, "Implementation of physical-layer network coding," *Physical Communication*, vol. 6, pp. 74 - 87, 2013.

[11] Y. Li, and L. J. Cimini, "Bounds on the interchannel interference of OFDM in time-varying impairments," *IEEE Trans. Commun.*, vol. 49, no. 3, 2001.

[12] I. W.-H. Ho, S. C. Liew, and L. Lu, "Feasibility study of physical-layer network coding in 802.11p VANETs," in *Proc. of IEEE ISIT*, 2014.

[13] L. F. Xie, I. W.-H. Ho, S. C. Liew, L. Lu, and F. C. M. Lau, "Mitigating Doppler effects on physical-layer network coding in VANET," in *Proc. of IEEE PIMRC*, 2015.

[14] L. Lu, and S. C. Liew, "Asynchronous physical-layer network coding," *IEEE Trans. Wireless Commun.*, vol. 11, no. 2, pp. 819 - 831, 2012.

[15] J. Yedidia, W. Freeman, and Y. Weiss, "Understanding belief propagation and its generalizations," *Technical Report TR2001-22*, MERL, 2001.

[16] E. D. N. Ndih, and S. Cherkaoui, "Toward neighborhood prediction using physical-layer network coding," in *Proc. of IEEE ICC*, pp. 676 - 680, 2012.

[17] E. Ndih, and S. Cherkaoui, "Mac for PNC in VANETs," *International Journal of Business Data Communications and Networking*, vol. 8, no. 4, pp. 84 - 106, 2012.

[18] M. Park, I. Choi, and I. Lee, "Exact BER analysis of physical-layer network coding for two-way relay channels," in *Proc. of IEEE VTC*, 2011.

[19] Y. Huang, S. Wang, Q. Song, L. Guo, and A. Jamalipour, "Synchronous physical-layer network coding: a feasibility study," *IEEE Trans. Wireless Commun.*, vol. 12, no. 8, pp. 4048 - 4057, 2013.

[20] T. Koike-Akino, P. Popovski, and V. Tarokh, "Optimized constellations for two-way wireless relaying with physical network coding," *IEEE J. Sel. Areas Commun.*, vol. 27, no. 5, pp. 773 - 787, 2009.

[21] S. Zhang, S. C. Liew, and H. Wang, "Synchronization analysis for wireless TWRC operated with physical-layer network coding," *Wireless Personal Communications*, Springer, vol. 68, no. 3, pp. 647-653, 2013.

[22] M. Wu, F. Ludwig, M. Woltering, D. Wubben, A. Dekorsy, and S. Paul, "Analysis and implementation for physical-layer network coding with carrier frequency offset," in *Proc. of ITG WSA*, pp. 1-8, 2014.

[23] M. Woltering, D. Wubben, and A. Dekorsy, "Physical layer network coding with Gaussian waveforms using soft interference cancellation," in *Proc. of VTC Spring*, 2015.

[24] T. Wang and S. C. Liew, "Joint channel estimation and channel decoding in physical-layer network coding systems: an EM-BP factor graph framework," *IEEE Trans. Wireless Commun.*, vol. 13, no. 4, pp. 2229 - 2245, 2014.

[25] T. Lv, H. Li, and J. Chen, "Joint estimation of symbol timing and carrier frequency offset of OFDM signals over fast time-varying multipath channels," *IEEE Trans. Signal Process.*, vol. 53, no. 12, pp. 4526 - 4535, 2005.

[26] Q. Yang and S. C. Liew, "Asynchronous convolutional-coded physical-layer network coding," *IEEE Trans. Wireless Commun.*, vol. 14, no. 3, pp. 1380 - 1395, 2015.

[27] G. Bartoli, R. Fantacci, D. Marabissi, and R. Simoni, "Subcarrier suppression methods for OFDM systems with decode-and-forward network coding," *IEEE Trans. Wireless Commun.*, vol. 12, no. 12, pp. 6034 - 6042, 2013.

[28] M. Stojanovic, "Low complexity OFDM detector for underwater acoustic channels," in *Proc. of IEEE OCEANS*, 2006.

[29] J. Zhu and W. Lee, "Carrier frequency offset estimation for OFDM systems with null subcarriers," *IEEE Trans. Vehicular Technology*, vol. 55, no. 5, pp.1677 - 1690, 2006.

[30] LitePoint, "Practical manufacturing testing of 802.11 OFDM wireless devices," *white paper*, 2012.

[31] V. Mhatre, "Enhanced wireless mesh networking for ns-2 simulator," *ACM SIGCOMM Computer Communication Review*, vol. 37, no. 3, 2007.

[32] M. Woltering, D. Wubben, A. Dekorsy, S. Schedler, and V. Kuhn, "Physical layer network coding using Gaussian waveforms: a link level performance analysis," in *Proc. of ITG SCC*, 2015.

Ling Fu Xie received his B. Eng. and M. Eng. in communications engineering from University of Electronic Science and Technology of China in 2006 and 2009, respectively, and his PhD degree from Nanyang Technological University, Singapore, in 2014. From 2014 to 2015, he worked as a post-doctoral fellow in The Hong Kong Polytechnic University, Hong Kong. In Oct. 2015, he joined the Faculty of Electrical Engineering and Computer Science of Ningbo University, Ningbo, China. His research interests mainly include protocol design and performance analysis in mobile networks, wireless network coding, and physical-layer network coding.

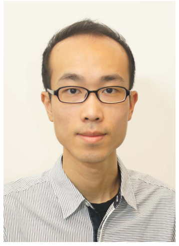

Ivan Wang-Hei Ho received the B.Eng. and M.Phil. degrees in information engineering from The Chinese University of Hong Kong, Shatin, Hong Kong, in 2004 and 2006, respectively, and the Ph.D. degree in electrical and electronic engineering from Imperial College London, London, U.K., in 2010. He is currently a Research Assistant Professor with the Department of Electronic and Information Engineering, The Hong Kong Polytechnic University, Kowloon, Hong Kong. He was with the Mobile Environmental Sensing System Across a Grid Environment (MESSAGE) project funded by the Engineering and Physical Sciences Research Council and the Department for Transport of the U.K., as well as with the International Technology Alliance project funded by the U.S. Army Research Laboratory and the Ministry of Defence of U.K. during his Ph.D. studies. In 2007, he spent a summer with the IBM Thomas J. Watson Research Center, Hawthorne, NY, USA. After his Ph.D. graduation, he was with the System Engineering Initiative, Imperial College London, as a Postdoctoral Research Associate. In September 2010, he cofounded P2 Mobile Technologies Ltd., Hong Kong Science Park, and served as the Chief R&D Engineer. He is also the holder of a U.S. patent. His publications can be found at http://www.eie.polyu.edu.hk/∼whho. His research interests are in wireless communications and networking, specifically in vehicular ad hoc networks and intelligent transportation systems, wireless mesh networks, internet of things, and physical-layer network coding. Dr. Ho primarily invented the MeshRanger series wireless mesh embedded system, which won the Silver Award in Best Ubiquitous Networking at the Hong Kong ICT Awards 2012.

Soung Chang Liew received the SB, SM, EE, and PhD degrees from the Massachusetts Institute of Technology. From 1984 to 1988, he was at the MIT Laboratory for Information and Decision Systems, where he investigated fiberoptic communications networks. From March 1988 to July 1993, he was at Bellcore (now Telcordia), New Jersey, where he engaged in Broadband Network Research. He has been a professor at the Department of Information Engineering, the Chinese University of Hong Kong, since 1993. He is an adjunct professor at Southeast University, China. His current research interests include wireless networks, Internet protocols, multimedia communications, and packet switch design. His research group won Best Paper Awards at IEEE MASS 2004 and IEEE WLN 2004. Separately, TCP Veno, a version of TCP to improve its performance over wireless networks proposed by his research group, has been incorporated into a recent release of Linux OS. In addition, he initiated and built the first inter-university ATM network testbed in Hong Kong in 1993. More recently, his research group pioneered the concept of Physical-layer Network Coding (PNC) for application in wireless networks. Besides academic activities, he is also active in the industry. He cofounded two technology startups in Internet software and has been serving as a consultant to many companies and industrial organizations. He is currently a consultant for the Hong Kong Applied Science and Technology Research Institute (ASTRI), providing technical advice as well as help to formulate R&D directions and strategies in the areas of wireless inter-networking, applications, and services. He received the first Vice-Chancellor Exemplary Teaching Award from the Chinese University of Hong Kong. His publications can be found at http://www.ie.cuhk.edu.hk/soung. He holds seven US patents and is a fellow of the IEEE, IEE, and HKIE.

Lu Lu received his B.E. from the University of Science and Technology of China (USTC) in 2007, and his Ph.D. from The Chinese University of Hong Kong (CUHK), in 2012. He was a postdoctoral fellow in the Institute of Network Coding (INC) from 2012 to 2014, and was a research assistant professor in the Institute of Network Coding (INC) from 2014 to 2017, at CUHK. Since 2016, he has been a researcher at the Technology and Engineering Center for Space Utilization (CSU), Chinese Academy of Science (CAS).

He is the recipient of the Faculty's Outstanding Ph.D. Thesis Award and the Postgraduate Research Output Award both in 2013 at CUHK. His research interests include wireless communications, multi-user detection, physical-layer network coding, and software-defined radios.

Francis C. M. Lau received the BEng (Hons) degree in electrical and electronic engineering and the PhD degree from King's College London, University of London, UK.

He is a Professor and Associate Head at the Department of Electronic and Information Engineering, The Hong Kong Polytechnic University, Hong Kong. He is a senior member of IEEE and a fellow of IET. He is the co-author of *Chaos-Based Digital Communication Systems* (Heidelberg: Springer-Verlag, 2003) and *Digital Communications with Chaos: Multiple Access Techniques and Performance Evaluation* (Oxford: Elsevier, 2007). He is a co-holder of four US patents and he has published over 270 papers, including over 120 journal publications. His main research interests include channel coding, cooperative networks, applications of complex-network theories, wireless sensor networks, chaos-based digital communications, and wireless communications.

He served as an associate editor for *IEEE Transactions on Circuits and Systems II (2004-2005)*, *IEEE Transactions on Circuits and Systems I (2006-2007)* and *IEEE Circuits and Systems Magazine (2012-2015)*. He has been a guest associate editor of *International Journal and Bifurcation and Chaos* since 2010, an associate editor of *IEEE Transactions on Circuits and Systems II* again since 2016. He was also the Chair of Technical Committee on Nonlinear Circuits and Systems, IEEE Circuits and Systems Society from 2012-2013 and the co-track chair of Nonlinear Circuits and Systems, 2010 IEEE International Symposium on Circuits and Systems.